Università di Padova

Dipartimento di Ingegneria dell'Informazione

Corso di Laurea Magistrale in Ingegneria delle Telecomunicazioni

Massive MIMO systems at millimeter-wave

Beamforming design and channel estimation

Studente

Stefano Montagner

Supervisore:

Prof. Nevio Benvenuto

Anno Accademico 2013/2014

Abstract

Millimeter-wave (MMW) is a probable technology for the future cellular systems. Its main challenge is achieving sufficient operating link margin, and directional beamforming with large antenna arrays may be a viable approach. With bandwidths on the order of gigahertz, high-resolution analog-to-digital converters are a power consumption bottleneck. One solution is to employ an hybrid implementation, digital at baseband and analog at radio frequencies.

In this thesis we develop three iterative hybrid beamforming design algorithms for the MMW channel, one using the channel structure, in particular the ray phase vector response and two using vector quantization of the analog beamformers. The proposed algorithms account for the RF precoding constraints and assumes the channel matrix is known. We compare the proposed algorithms with the state-of-art hybrid schemes and the simulation results show that performance of the proposed algorithms can approximate that of the maximum-ratio-beamforming upper bound even if computational complexity may be higher for low number of antennas.

Within this framework, channel estimation plays a fundamental role for the system design. By exploiting the limited scattering structure of the MMW channel across the numerous antennas, and by using a suitable training sequence of symbols at the transmitter, we develop two algorithms that estimate the channel parameters at the receiver directly, rather than the multiantenna channel matrix. Moreover, the algorithms account for the analog precoder/beamformer constraint. Furthermore our approach does not require a feedback from the transmitter. By extensive simulations it is seen that the algorithms are quite simple, very robust, and yield very good performance, close to the case of perfect channel knowledge.

Contents

Notation

Symbol	Description
$\mathbf{a}$	Column vector $\mathbf{a}$ (boldface lower-case letter)
$\mathbf{A}$	Matrix $\mathbf{A}$ (boldface capital letter)
$row_i(\mathbf{A})$	The row i of matrix $\mathbf{A}$
$col_j(\mathbf{A})$	The column j of matrix $\mathbf{A}$
$[\mathbf{A}]_{i,j}$	The entry on row i and column j of matrix $\mathbf{A}$
$[\mathbf{y}]_{a:b}$	Vector obtained extracting elements from index 'a' to 'b'
$\mathbf{A}^T$	Transpose of $\mathbf{A}$
$\mathbf{A}^H$	Conjugate transpose (Hermitian) of $\mathbf{A}$
$\mathbf{I}_n$	$n \times n$ identical matrix
$diag(a_1, a_2, ..., a_n)$	$n \times n$ diagonal matrix with $a_1, a_2, ..., a_n$ its main diagonal
$tr(\mathbf{A})$	Trace of $\mathbf{A}$
$vert(\mathbf{A})$	Verticalization of matrix $\mathbf{A}$ for columns
a^*	Conjugate of scalar a
$\angle(a)$	Angle value of scalar a
$\|a\|$	Amplitude of scalar a
$\|\|\mathbf{a}\|\|$	Two-norm of vector $\mathbf{a}$ (Euclidean norm)
$\|\|\mathbf{A}\|\|$	Two-norm of matrix $\mathbf{A}$ (Euclidean norm)
a_M	Maximum value taken by real scalar a
$\mathbb{E}[\cdot]$	Expected value
$\bar{x} = \mathbb{E}[x]$	Mean of random variable x
$M_x = \mathbb{E}[\|x\|^2]$	Statistical power of random variable x
$\sigma_x^2 = \mathbb{E}[\|x - \bar{x}\|^2]$	Variance of random variable x

List of acronyms

MMW	mm-waves
Tx	transmitter
Rx	receiver
UHF	ultra high frequencies
ULA	uniform linear array
LOS	line on sight
SNR	signal to noise ration
i.i.d.	independent identically distributed
RF	radio frequency
BB	base-band
ADC	analog to digital converter
DAC	digital to analog converter
SVD	singular value decomposition
AWGN	additive white Gaussian noise
SISO	single input single output
MIMO	multiple input multiple output
MISO	multiple input single output
SIMO	single input multiple output
MRB	maximum ratio beamforming
I-MRB	iterative maximum ratio beamforming
ADB	analog-digital beamforming
I-ADB	iterative analog-digital beamforming
Q-ADB	quantized analog-digital beamforming
QI-ADB	quantized iterative analog-digital beamforming
DFT	discrete fourier transform
2D-DFT	two-dimensional discrete fourier transform
VQ	vector quantization
SQ	scalar quantization
LBG	Linde, Buzo and Gray algorithm
TS	training sequence

Introduction

Millimeter-wave (MMW) communication is a promising technology for future outdoor cellular systems [1],[2],[3]. This technology provide gigabit-per-second data rates in a bandwidth between 30 and 300 GHz. Overall it has the potential to unleash very high data rates even if with low spectral efficiencies. However MMW systems must counter the strong attenuation introduced by the radio link. On the other hand, the millimeter wavelength allows the use of arrays with a large number of antennas in transmission and in reception, hence we can combat the transmission path loss with highly directional beamforming. Conventional multiple-input multiple-output (MIMO) systems require all the antenna paths to be independently acquired and jointly processed at the baseband. This increases the cost of the transceiver, which is approximately proportional to the number of analog-to-digital converters (ADCs) [4],[5]. For this reason, the implementation of conventional MIMO transceivers becomes a major problem in low-cost wireless terminals, where the hardware complexity is strictly limited. To increase the performance of such systems without excessively increasing the size and hardware cost, several proposed schemes shift part of the spatial signal processing from the baseband to the radio-frequency (RF) front-end [6],[7],[8]. In this thesis, we focus on the transmit and receive beamforming and in particular on solutions that can be derived from jointly considering the three factors: RF beamforming constraints, large antenna arrays, and limited digital processing capability due to its high power consumption. We adopt a realistic finite ray channel model which captures both the limited scattering at high frequency and the antenna correlation of large arrays. Within this framework, in [8] a hybrid analog-digital, denoted analog-digital beamforming (ADB), solution is proposed, where the antenna array is driven by a limited number of RF chains and multiantenna processing is implemented via a combined RF analog and baseband digital solution.
Unfortunately the design of ADB has a high computational complexity. To reduce this cost we have proposed iterative-ADB (I-ADB) which make use of the channel structure, in particular the ray phase vector response, to design the analog beamformer and a iterative algorithm to design the digital-beamformer. It is seen that this algorithm has a much lower computational complexity and achieves a perfor-

mance close to the ADB.
ADB and I-ADB design methods require to acquire each ray phase vector response. To reduce further of the computational complexity we have vector quantized the values of analog beamformers. Corresponding by for the beamformer design we have implemented two algorithms: the first, denoted quantized analog digital beamforming (Q-ADB), readjusts the analog-digital beamforming (ADB) algorithm [8] in the presence of vector quantized analog beamformers, the second, denoted quantized iterative analog digital beamforming (QI-ADB), is a suboptimal algorithm which iteratively design the transmit and receive digital beamformers once we explore the analog beamformers by a precomputed codebook. It is seen that QI-ADB has a much lower computational complexity than Q-ADB. Based on the channel knowledge, as for [9], we evaluate performance, in terms of signal to noise ratio (SNR) at detection point, of the two algorithms through simulations. Moreover we also report the computational complexity of both algorithms and compare it with that of ADB. The results show that two algorithms performs close to the maximum-ratio-beamforming upper bound, using a lower computational complexity than that of ADB.
The last problem we considered was the channel estimate within the ADB framework, we recall the procedure [9], where the channel estimate, given by a prestored hierarchical codebook, is obtained by iterative design of the precoder/beamformer done, respectively, at transmitter and receiver. The main problem of this method is that it requires a feedback channel for the iterative exchange of information between transmitter and receiver. A more classical approach of MIMO channel estimate is proposed in [11] where the channel matrix is directly estimated by a suitable training sequence. However this method cannot be extended to the hybrid precoder/beamformer structure. Moreover its complexity would be very high considering that we may have up to hundreds of transmit/receive antennas. In fact, a contribution of our approach is to realize that the channel matrix depends upon very few parameters, hence it is simpler to estimate these parameters rather than the channel matrix. Moreover, the relationship between these parameters and the channel matrix is very simple in the frequency domain, i.e. by taking the discrete Fourier transform of the signal across the receiver antennas.
Differently from previous approaches we develop a specific training sequence of precoders and beamformers in order to estimate the channel parameters. Once these parameters are estimated, we can i) reconstruct the elements of the channel matrix and ii) design the transmit precoder and receive beamformer using the I-ADB algorithm [8]. For this scope we have proposed two different method, the first based on a Discrete Fourier Transform (DFT) and the second using a Two-Dimensional DFT (2D-DFT).
The results show that our algorithms achieves good performance, very close to the

case of perfect channel knowledge especially by using the 2D-DFT channel estimation.

Chapter 1

Channel model

Compared to lower bands, radio waves in millimeter band have high atmospheric attenuation and are blocked by building walls and attenuated by foliage, which can be a limiting impairment for propagation in some cases. On the other hand for the same antenna aperture areas, shorter wavelengths should not have any inherent disadvantage compared to longer wavelengths in terms of free space loss. More antennas can be packed into the same area if the wave length is small, allowing beamforming with high gains. In this chapter we analize the multiple input multiple output (MIMO) channel model.

1.1 Channel impulse response

The equivalent complex base band impulse response of a MMW MIMO channel with narrow-band impulses is a matrix $\mathbb{C}^{N\times M}$, where M is the number of antennas at transmitter (Tx) and N is the number of antennas at receiver (Rx).

$$\mathbf{H} = \sqrt{G}\begin{bmatrix} h_{1,1} & \cdots & h_{1,M} \\ \vdots & \ddots & \vdots \\ h_{N,1} & \cdots & h_{N,M} \end{bmatrix} \tag{1.1}$$

where G is the mean gain of channel. The element of $\mathbf{H}$ are complex random variables and the matrix should satisfies the average constraint on its squared Frobenius norm

$$\mathbb{E}\left[||\mathbf{H}||^2\right] = MN. \tag{1.2}$$

1.2 MIMO channel model

The reference model for the MIMO channel is used where we have a limited spatial diversity and for a high number of antennas in the same area, as in the case of MMW.

This model is taken from [8, pp. 3783] and describes a channel matrix for an uniform linear array (ULA) for beamforming in azimuth plane and for a uniform planar array uniform planar array (UPA) which enables beamforming also in elevation.

Uniform linear array

Let us consider antenna elements to form an ULA on the azimuth plane with an inter-element spacing equal to D. For a uniform linear array with N elements, let $\mathbf{a}$ be a column vector of phasors

$$\mathbf{a}(\phi) = \begin{bmatrix} 1 & e^{j\zeta D \sin\phi} & \dots & e^{j(N-1)\zeta D \sin\phi} \end{bmatrix}^T \tag{1.3}$$

where $\zeta = 2\pi/\lambda$ and ϕ represents the angle of arrival for the receiver, or the angle of starting for the transmitter in the azimuth plane. With the assumption that L rays are received with the same delay, the channel vector is given by

$$\mathbf{H} = \frac{1}{\sqrt{L}} \sum_{\ell=1}^{L} g_\ell \mathbf{a}_r\left(\phi_\ell^{(r)}\right) \mathbf{a}_t^H\left(\phi_\ell^{(t)}\right) \tag{1.4}$$

where L is the total number of rays and $g_\ell \sim \mathcal{CN}(0,1)$ represents the complex random gain of the ℓ-th ray. Note that the elements of $\mathbf{a}(\phi)$ represent phase offsets due to distances between antenna elements. The relative phase difference for a ULA is a function only of the azimuth variable ϕ. Moreover, in (1.4) the average gain factor $\sqrt{G}$ is dropped for simplicity.

Matrix formulation

The expressions of MIMO channel impulse response given in (1.4) can be rewritten [12, p. 27] into a useful matrix form:

$$\mathbf{H} = \frac{1}{\sqrt{L}} \mathbf{A}_r \mathbf{H}_q \mathbf{A}_t^H \tag{1.5}$$

where

$$\begin{aligned} \mathbf{A}_t &= \begin{bmatrix} \mathbf{a}_t\left(\phi_1^{(t)}\right) & \mathbf{a}_t\left(\phi_2^{(t)}\right) & \dots & \mathbf{a}_t\left(\phi_L^{(t)}\right) \end{bmatrix} \\ \mathbf{A}_r &= \begin{bmatrix} \mathbf{a}_r\left(\phi_1^{(r)}\right) & \mathbf{a}_r\left(\phi_2^{(r)}\right) & \dots & \mathbf{a}_r\left(\phi_L^{(r)}\right) \end{bmatrix} \\ \mathbf{H}_g &= diag(g_1, g_2, ..., g_L) \end{aligned} \tag{1.6}$$

The correlation of ULA channel

In this section we reported, from [21], an expression for the entries of the ULA Tx and Rx channel correlation matrices,

$$\mathbf{R}_{TX} = \mathbb{E}\left[\mathbf{H}^H\mathbf{H}\right] \qquad and \qquad \mathbf{R}_{RX} = \mathbb{E}\left[\mathbf{H}\mathbf{H}^H\right] \tag{1.7}$$

Applying the expectation, we are able to provide a closed form expression for the generic entry on row p and column q of the Tx correlation matrix

$$[\mathbf{R}_{TX}]_{p,q} = \frac{N}{\phi_{max} - \phi_{min}} \int_{\phi_{min}}^{\phi_{max}} e^{j\zeta(p-q)\sin a} da \tag{1.8}$$

and of the Rx correlation matrix

$$[\mathbf{R}_{TX}]_{p,q} = \frac{M}{\phi_{max} - \phi_{min}} \int_{\phi_{min}}^{\phi_{max}} e^{j\zeta(p-q)\sin a} da \tag{1.9}$$

We note that the amplitude of the correlation matrix entries are independent of the number of rays L of the ULA channel model.

Numerical examples of ULA correlation matrix

A couple of numerical examples for the amplitude of (1.8) with $\phi_{min} = -60°$, $\phi_{max} = 60°$, wavelength $\lambda = 0.005m$, $M = 6$ are given with an antenna separation $D = \lambda/2$:

$$abs\left(\frac{\mathbf{R}_{TX}}{N}\right) = \begin{bmatrix} 1 & 0.03 & 0.13 & 0.15 & 0.14 & 0.11 \\ 0.03 & 1 & 0.03 & 0.13 & 0.15 & 0.14 \\ 0.13 & 0.03 & 1 & 0.03 & 0.13 & 0.15 \\ 0.15 & 0.13 & 0.03 & 1 & 0.03 & 0.14 \\ 0.14 & 0.15 & 0.13 & 0.03 & 1 & 0.03 \\ 0.11 & 0.14 & 0.15 & 0.13 & 0.03 & 1 \end{bmatrix} \tag{1.10}$$

and $D = \lambda/5$:

$$abs\left(\frac{\mathbf{R}_{TX}}{N}\right) = \begin{bmatrix} 1 & 0.78 & 0.28 & 0.16 & 0.30 & 0.13 \\ 0.78 & 1 & 0.78 & 0.28 & 0.16 & 0.30 \\ 0.28 & 0.78 & 1 & 0.78 & 0.28 & 0.16 \\ 0.16 & 0.28 & 0.78 & 1 & 0.78 & 0.28 \\ 0.30 & 0.16 & 0.28 & 0.78 & 1 & 0.78 \\ 0.13 & 0.30 & 0.16 & 0.28 & 0.78 & 1 \end{bmatrix} \tag{1.11}$$

We observe that by increasing D leads to a decreasing correlation between elements.

1.3 Simulation of the ULA channel

For the simulation results we use a typical $60GHz$ channel with $L = 3$ rays and carrier with a wave length of $\lambda = 0.005m$. The Rx and Tx ULA arrays are made of antenna elements separated by $D = \lambda/2$. The angle of arrival and departure are random uniformly distributed in the interval between $\phi_{min} = -60^\circ$ and $\phi_{max} = 60^\circ$.

Chapter 2

Optimal and sub-optimal beamforming

At the beginning of this chapter we introduce the general framework for the performance analysis, in terms of signal to noise ratio (SNR), of a MMW MIMO system. Next we discuss, from a theoretical point of view, the state of art and various sub-optimal array gain techniques for conventional MIMO systems.

2.1 SNR definitions

We introduce various definitions of SNR that are used later to evaluate and compare the performance of the systems considered. We start by defining the average SNR, with respect to noise and channel gain, of a simple single input single output (SISO) system denoted here additive white Gaussian noise (AWGN) channel. Next, we extend the definition of SNR for a MIMO system.

2.1.1 AWGN channel

Figure 2.1 shows the base-band equivalent of a flat-fading AWGN channel system, where x denotes the information symbol and y the received symbol at decision point equal to

$$y = hx + n \tag{2.1}$$

where the noise, n, is Gaussian distributed with zero mean and variance σ_n^2,

$$n \sim \mathcal{CN}\left(0, \sigma_n^2\right) \tag{2.2}$$

We denote with

$$\mathtt{M}_h = \mathbb{E}[|h|^2], \qquad \mathtt{M}_x = \mathbb{E}[|x|^2] \tag{2.3}$$

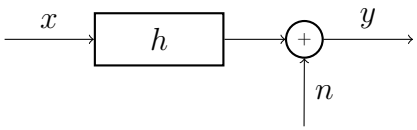

Figure 2.1: AWGN system: base band equivalent scheme.

the statistical power of the channel gain h and the information symbol x respectively. The expression of the average SNR at receiver, called Γ_{AWGN}, is given by

$$\Gamma_{AWGN} = \frac{\mathbb{E}_{h,x}[|hx|^2]}{\mathbb{E}_n[|n|^2]} = \frac{\mathbb{E}_h[|h|^2]\mathbb{E}_x[|x|^2]}{\sigma_n^2} = \frac{\mathtt{M}_h\mathtt{M}_x}{\sigma_n^2} \tag{2.4}$$

Setting the statistical power of the input sample and of the channel to one

$$\mathtt{M}_h = \mathtt{M}_x = 1 \tag{2.5}$$

yields

$$\Gamma_{AWGN} = \frac{1}{\sigma_n^2} \tag{2.6}$$

2.1.2 MIMO channel

We consider now a generic MIMO configuration with M antennas at the transmitter and N antennas at the receiver. We provide a SNR definition associated to a specific channel realization and averaged with respect to the noise contribution. Moreover, we define a functional that measures the improvement, in terms of SNR, of the MIMO system with respect to the AWGN case.

System model

Figure 2.2 shows the system considered and the precoder and combiner elements. where x denotes the information symbol, y the received symbol, $\mathbf{s}$ the transmitted signal vector and $\mathbf{r}$ the received signal vector. The received vector noise $\mathbf{n}$ is modelled as a complex circular independent identically distributed (i.i.d.) Gaussian noise vector,

$$\mathbf{n} \sim \mathcal{CN}\left(0, \sigma_n^2 \mathbf{I}_N\right) \tag{2.7}$$

where σ_n^2 is the variance of the generic entry of $\mathbf{n}$, which is distributed as (2.2), and $\mathbf{I}_N$ the $N \times N$ identity matrix.

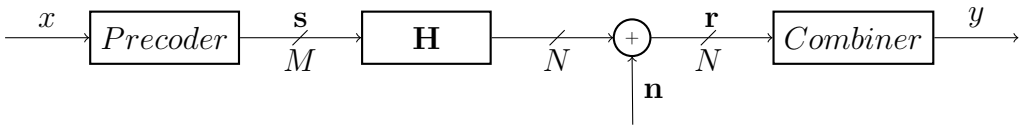

Figure 2.2: MIMO system: base band equivalent scheme.

SNR expression

At the decision point, for a given channel realization $\mathbf{H}$, after the combining operation of received signals, we consider the SNR, expressed by Γ, as the ratio between the statistical power of useful part of the signal and the statistical power of the noise component. Next we normalize Γ to the channel noise and define the metric

$$\gamma = \frac{\Gamma}{\Gamma_{AWGN}} \tag{2.8}$$

Moreover we will characterize the system performance on average with respect to the channel and define

$$\bar{\Gamma} = \mathbb{E}_{\mathbf{H}}[\Gamma], \quad \bar{\gamma} = \mathbb{E}_{\mathbf{H}}[\gamma] = \frac{\bar{\Gamma}}{\Gamma_{AWGN}} \tag{2.9}$$

where $\mathbb{E}_{\mathbf{H}}[\cdot]$ denotes that the expectation is taken with the respect to the channel $\mathbf{H}$.

2.2 Optimal beamforming

We seek now to design the optimal precoder and combiner of Figure 2.2 in order to maximize γ in (2.8). We will see that the optimal solution is represented, both at Tx and Rx side, by the maximum ratio beamforming (MRB).
The precoder and combiner in Figure 2.2 are substituted by two vectors of weights called beamformers. Let

$$\boldsymbol{f} = [f_1, ..., f_M]^T \quad and \quad \boldsymbol{u} = [u_1, ..., u_N]^T \tag{2.10}$$

be the transmit and receive beamformers. The input stream modulates the Tx antennas array by the weights of $\boldsymbol{f}$, while the vector signal at the receiver antenna array is recombined to an output single stream by weight vector $\boldsymbol{u}$. Figure 2.3 represents the described system. The transmitted vector signal $\mathbf{s}$ is represented by the entries

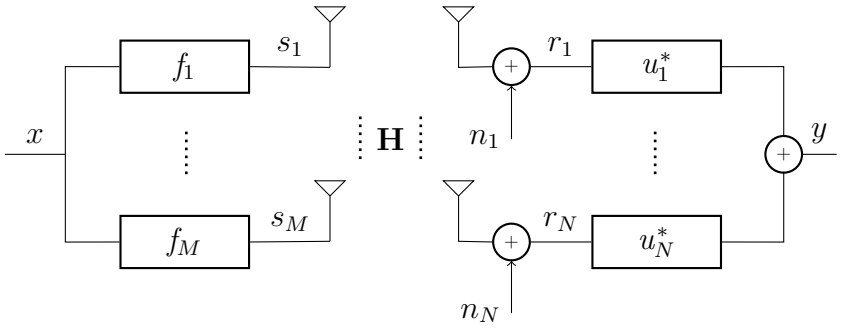

Figure 2.3: MRB system: base band equivalent scheme.

$$\mathbf{s} = [s_1, ..., s_M]^T \tag{2.11}$$

and its expression is

$$\mathbf{s} = \boldsymbol{f}x \tag{2.12}$$

We note that if the transmitted signal $\mathbf{s}$ is subject to an average power constraint P it implies that also the power of the beamformer $\boldsymbol{f}$ is constrained and it must be,

$$\mathbb{E}_x[||\mathbf{s}||^2] = ||\boldsymbol{f}||^2 \mathtt{M}_x \leq P \quad \Longrightarrow \quad ||\boldsymbol{f}||^2 \leq \frac{P}{\mathtt{M}_x} \tag{2.13}$$

The received signal $\mathbf{r}$ is denoted by the vector

$$\mathbf{r} = [r_1, ..., r_N]^T \tag{2.14}$$

and it is equal to

$$\mathbf{r} = \mathbf{H}\boldsymbol{f}x + \mathbf{n} \tag{2.15}$$

2.2.1 SNR expression

The reconstructed signal y is equal to

$$y = \boldsymbol{u}^H \mathbf{H}\boldsymbol{f}x + \boldsymbol{u}^H \mathbf{n} \tag{2.16}$$

where $\mathbf{n}$ is defined in (2.7).
Without loss of generality, let us consider x with unitary average power ($\mathtt{M}_x = 1$) and a transmission power constraint $P = 1$. Hence from (2.13) it must be $||\boldsymbol{f}||^2 = 1$. Moreover we assume a unit statistical power for each entry of the channel matrix $\mathbf{H}$, as from (2.5). If also the power of the combiner is equal to one ($||\boldsymbol{u}||^2 = 1$) from (2.16) we can provide the expression of

$$\Gamma = \frac{\mathbb{E}_x[|\boldsymbol{u}^H \mathbf{H}\boldsymbol{f}|^2]}{|\boldsymbol{u}^H \mathbf{n}|^2} = \frac{|\boldsymbol{u}^H \mathbf{H}\boldsymbol{f}|^2}{\sigma_n^2} \tag{2.17}$$

and (2.8) becomes

$$\gamma = |\boldsymbol{u}^H \mathbf{H} \boldsymbol{f}|^2. \tag{2.18}$$

2.2.2 The optimization problem

We focuse now on finding weight vectors $\boldsymbol{f}$ and $\boldsymbol{u}$ that maximize the functional (2.18). The optimization problem can be outlined as

$$\begin{aligned} &\max_{\boldsymbol{f},\boldsymbol{u}} |\boldsymbol{u}^H \mathbf{H} \boldsymbol{f}|^2 \\ &with \quad ||\boldsymbol{f}||^2 = 1, \quad ||\boldsymbol{u}||^2 = 1. \end{aligned} \tag{2.19}$$

The constraints on the squared norm of the beamformers suggest that γ should be maximized by choosing the optimal $\boldsymbol{f}$ and $\boldsymbol{u}$ with no increase of the needed power.

2.3 Maximum ratio beamforming (MRB)

The solution of problem (2.19) is well known in the literature [15, pp. 44] and implies the singular value decomposition (SVD) of channel matrix $\mathbf{H}$. In the next section we briefly summarize the procedure and outline the maximum value reached by γ for a given channel, next, some numerical values of $\bar{\gamma}$ will be given.

2.3.1 The SVD solution

The complex $N \times M$ channel matrix $\mathbf{H}$ with rank ρ has the following SVD decomposition [15]

$$\mathbf{H} = \mathbf{U}\boldsymbol{\Xi}\mathbf{F} = \begin{bmatrix} \boldsymbol{u}_1 & \dots & \boldsymbol{u}_N \end{bmatrix} \begin{bmatrix} \xi_1 & \dots & 0 \\ \vdots & \ddots & \vdots \\ 0 & \dots & \xi_\rho \\ 0 & \dots & 0 \\ \vdots & \ddots & \vdots \\ 0 & \dots & 0 \end{bmatrix} \begin{bmatrix} \boldsymbol{f}_1^H \\ \dots \\ \boldsymbol{f}_M^H \end{bmatrix} \tag{2.20}$$

where

- the non-zero diagonal real values of $\boldsymbol{\Xi} \in \mathbb{R}^{N \times M}$ are called singular values of $\mathbf{H}$ and they satisfy
$$\xi_1 \geq \xi_2 \geq ... \geq \xi_\rho \geq 0, \tag{2.21}$$
- the column vectors of $\mathbf{U} \in \mathbb{C}^{N \times N}$, denoted by $\boldsymbol{u}_1, ..., \boldsymbol{u}_N$ are the left singular vectors of $\mathbf{H}$,

- the column vectors of $\mathbf{F} \in \mathbb{C}^{M \times M}$, denoted by $\boldsymbol{f}_1, ..., \boldsymbol{f}_M$ are the right singular vectors of $\mathbf{H}$,

The complex matrices $\mathbf{U}$ and $\mathbf{F}$ are said to be unitary, which entails

$$\mathbf{U}^H\mathbf{U} = \mathbf{U}\mathbf{U}^H = \mathbf{I}_N, \quad \mathbf{F}^H\mathbf{F} = \mathbf{F}\mathbf{F}^H = \mathbf{I}_M. \tag{2.22}$$

It can be shown that the optimal beamformers for the problem (2.19), denoted by $\boldsymbol{f}_{MRB}$ and $\boldsymbol{u}_{MRB}$ are equal to the right singular vector associated to the largest singular value and to the left singular vector associated to the largest singular value, respectively. In symbols

$$\boldsymbol{f}_{MRB} = \boldsymbol{f}_1, \quad \boldsymbol{u}_{MRB} = \mathbf{u}_1 \tag{2.23}$$

We note that the constraints on the squared norms of beamformers are satisfied as from (2.22)

$$||\boldsymbol{f}_1||^2 = tr(\boldsymbol{f}_1^H\boldsymbol{f}_1) = 1, \quad ||\boldsymbol{u}_1||^2 = tr(\boldsymbol{u}_1^H\boldsymbol{u}_1) = 1 \tag{2.24}$$

2.3.2 Performance results

Performance, in terms of $\bar{\gamma}$, are evaluated by averaging (2.18) for 5000 realizations of the channel. Fig. 2.4 shows the average SNR improvement $\bar{\gamma}$ versus the number of antennas (number of Rx and Tx antennas is equal, i.e. $M = N$) for the MRB approach. We can see that $\bar{\gamma}$ saturates for high number of antennas, this is due to the fact that we use a finite ray channel model.

2.4 Iterative maximum ratio beamforming (I-MRB)

Applying the SVD of the channel matrix, the MRB provides a solution, in closed form, to the problem in (2.19) We investigate now an iterative approach to get the same solution [13]. For multiple input single output (MISO) ($N = 1$) or single input multiple output (SIMO) ($M = 1$) systems, the optimal solution to (2.19) is provided by simple expressions known in literature as maximum ratio transmission and maximum ratio reception. Part of the work in [13] exploits the simple MISO and SIMO solutions cyclically, in a procedure that converges in few iterations ($3 \div 7$) to the MRB performance.

2.4.1 Splitting and reformulation of the problem

Assuming that optimal $\boldsymbol{f}$ or, alternatively, $\boldsymbol{u}$ is known, problem (2.19) can be splitted into an iterative SIMO and MISO optimization problem. Let us set

$$\mathbf{h}_{SIMO} = \mathbf{H}\boldsymbol{f} \in \mathbb{C}^{N \times 1} \quad and \quad \mathbf{h}_{MISO} = \boldsymbol{u}^H\mathbf{H} \in \mathbb{C}^{1 \times M} \tag{2.25}$$

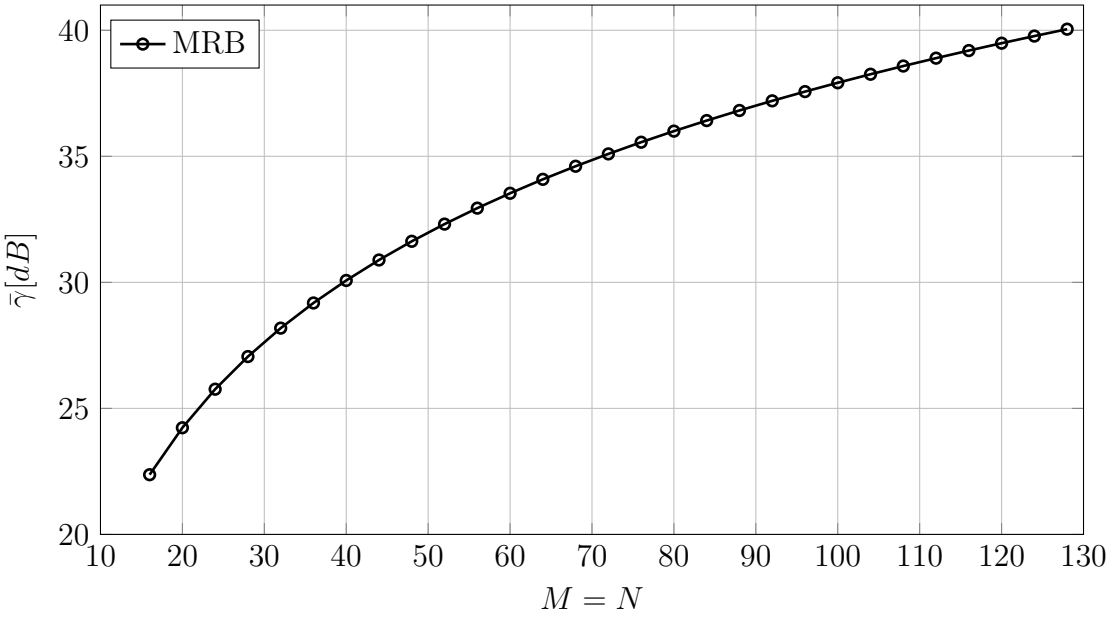

Figure 2.4: $\bar{\gamma}$ vs. M (and $M = N$) for the MRB approach.

The SIMO and MISO optimization problems are, respectively, expressed by

$$\begin{aligned} SIMO: \quad & \arg\max_{\boldsymbol{u}} |\boldsymbol{u}^H \mathbf{h}_{SIMO}|^2 \qquad MISO: \quad \arg\max_{\boldsymbol{f}} |\mathbf{h}_{MISO}\boldsymbol{f}|^2 \\ with \quad & ||\boldsymbol{u}||^2 = 1. \qquad with \quad ||\boldsymbol{f}||^2 = 1. \end{aligned} \tag{2.26}$$

The optimal solutions $\boldsymbol{f}_{I-MRB}$ and $\boldsymbol{u}_{I-MRB}$ can be shown ([13, p. 5396], [14, p. 1459]) to be equal to

$$\boldsymbol{f}_{I-MRB} = \frac{\mathbf{h}_{MISO}^H}{||\mathbf{h}_{MISO}||} \quad and \quad \boldsymbol{u}_{I-MRB} = \frac{\mathbf{h}_{SIMO}}{||\mathbf{h}_{SIMO}||} \tag{2.27}$$

2.4.2 Cyclic optimization procedure

The original SNR maximization problem in (2.19) is based on the fundamental assumptions made in (2.25) that imply the knowledge, a priori, of the optimum at transmitter and receiver for the SIMO or MISO problem, respectively. In order to bypass this issue, [13, p. 5398] proposes a simple cyclic procedure that can be described in few steps.

step 0 Set $\boldsymbol{u}$ to an initial value, for example a vector where entries are all equals to $1/\sqrt{N}$;

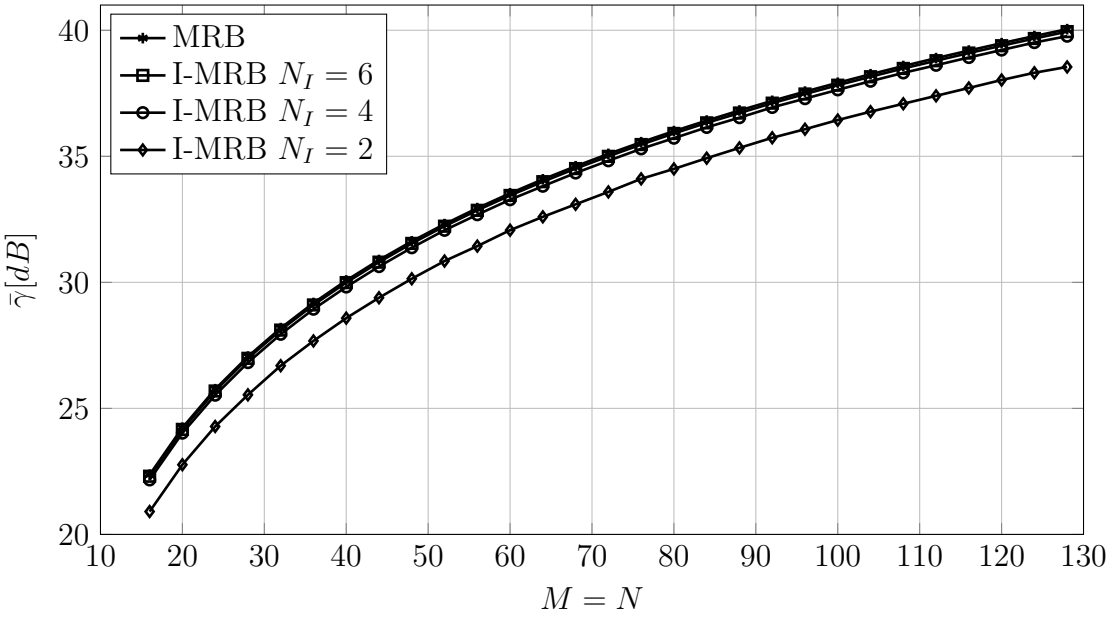

Figure 2.5: $\bar{\gamma}$ vs. M (and $M = N$) for the I-MRB approach.

step 1 obtain the transmitter beamformer $\boldsymbol{f}$ by solving the MISO problem in (2.27), setting $\mathbf{h}_{MISO} = \boldsymbol{u}_{I-MRB}^H \mathbf{H}$, where $\boldsymbol{u}$ is fixed at its most recent value;

step 2 update the receiver beamformer $\boldsymbol{u}$ by solving the SIMO problem in (2.27), setting $\mathbf{h}_{SIMO} = \mathbf{H}\boldsymbol{f}_{I-MRB}$, where $\mathbf{f}$ was obtained in *step 1*;

step 3 iterate *step 1* and *step 2* until a given stop criterion is satisfied.

2.4.3 Performance results

Performance, in terms of $\bar{\gamma}$, are evaluated by averaging (2.18) for 5000 realizations of the channel. This algorithm is simple and numerical simulations show that it converges in $N_I = 3 \div 7$ iterations. For a comparison we also report the MRB bound. Fig. 2.5 shows the average SNR improvement $\bar{\gamma}$ versus the number of antennas (number of Rx and Tx antennas is equal, i.e. $M = N$) for three values of N_I using the I-MRB approach.

2.5 Analog-digital beamforming (ADB)

Until now, only weight vector beamformers have been considered. Looking for alternative hardware configuration, which require loss power, in a MMW scenario, working in the RF domain could be more convenient, but, often, we lose the digital

base-band flexibility. Hence we investigate a analog-digital beamforming (ADB) layered architecture that is simpler to implement in the analog domain because it has a reduced number, with respect to the antenna elements, of RF chains. However, this configurations includes a base-band (BB) precoder and combiner in order to achieve MRB performance.

2.5.1 Framing of the problem

The analog-digital beamforming configuration is illustrated in Fig. 2.6, as from [8]. It models a single user MMW system, in which a single transmitter (Tx) with M antennas communicates symbol x to a single receiver (Rx) with N antennas and it consists of a transmitter equipped with M_{RF} radio frequency (RF) chains, with $M_{RF} < M$, and a receiver with N_{RF} RF chains, with $N_{RF} < N$. The transmitter is assumed to apply an $M_{RF} \times 1$ complex valued base-band digital precoder,

$$\mathbf{f}_{BB} = [f_{BB,1}, ..., f_{BB,M_{RF}}] \in \mathbb{C}^{M_{RF} \times 1}, \tag{2.28}$$

followed by a RF analog precoder

$$\mathbf{F}_{RF} = \begin{bmatrix} f_{1,1} & \dots & f_{1,M_{RF}} \\ \vdots & \ddots & \vdots \\ f_{M,1} & \dots & f_{M,M_{RF}} \end{bmatrix} \in \mathbb{C}^{M \times M_{RF}}. \tag{2.29}$$

Similarly, the receiver is constituted by a RF analog combiner

$$\mathbf{U}_{RF} = \begin{bmatrix} u_{1,1} & \dots & u_{1,N_{RF}} \\ \vdots & \ddots & \vdots \\ u_{N,1} & \dots & u_{N,N_{RF}} \end{bmatrix} \in \mathbb{C}^{N \times N_{RF}}. \tag{2.30}$$

and a base-band digital combiner

$$\mathbf{u}_{BB} = [u_{BB,1}, ..., u_{BB,N_{RF}}] \in \mathbb{C}^{N_{RF} \times 1}. \tag{2.31}$$

To simplify the hardware implementation, each element of $\mathbf{U}_{RF}$ and $\mathbf{F}_{RF}$ has unitary magnitude, whoever it may have an arbitrary phase. If $\mathbf{H}$ denotes the $N \times M$ channel matrix, let

$$\mathbf{x}_{BB} = \mathbf{f}_{BB} x \tag{2.32}$$

and defining

$$\mathbf{y}_{BB} = \mathbf{U}_{RF}^{H} (\mathbf{H}\mathbf{F}_{RF}\mathbf{x}_{BB} + \mathbf{n}) \tag{2.33}$$

the received signal can be written as

$$y = \mathbf{u}_{BB}^{H} \mathbf{y}_{BB} \tag{2.34}$$

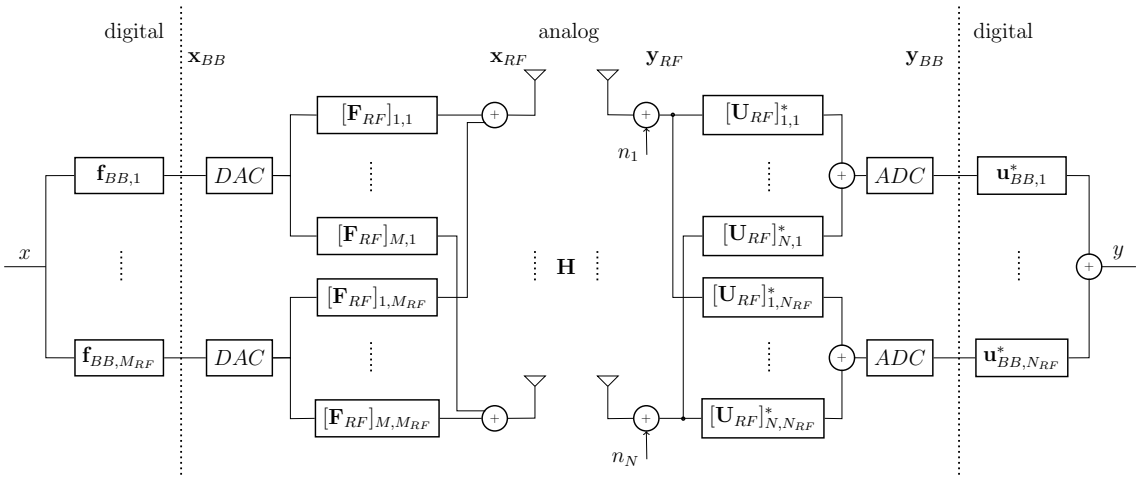

Figure 2.6: ADB system: base band equivalent scheme.

where $\mathbf{n} \sim \mathcal{CN}(0, \sigma_n^2 \mathbf{I}_N)$ with σ_n^2 the channel noise variance and $\mathbf{I}_N$ the $N \times N$ identity matrix. For later we also define the transmit and receive antenna signals, $\mathbf{x}_{RF} = \mathbf{F}_{RF}\mathbf{x}_{BB}$ and $\mathbf{y}_{RF} = \mathbf{H}\mathbf{x}_{RF} + \mathbf{n}$. We stress that in the ADB structure we only have access to signals $\mathbf{x}_{BB}$ and $\mathbf{y}_{BB}$, besides, obviously, to x and y, however we can switch on and off any antenna at transmitter/receiver.

2.5.2 SNR at detection point

From (2.34), for a given channel matrix and by assuming $||\mathbf{U}_{RF}\mathbf{u}_{BB}|| = 1$, we can define the *SNR at detection point* as

$$\Gamma = \frac{\mathbb{E}_x\left[\left|\mathbf{u}_{BB}^H \mathbf{U}_{RF}^H \mathbf{H}\mathbf{F}_{RF}\mathbf{f}_{BB}x\right|^2\right]}{\mathbb{E}_{\mathbf{n}}\left[\left|\mathbf{u}_{BB}^H \mathbf{U}_{RF}^H \mathbf{n}\right|^2\right]} = \left|\mathbf{u}_{BB}^H \mathbf{U}_{RF}^H \mathbf{H}\mathbf{F}_{RF}\mathbf{f}_{BB}\right|^2 \frac{\sigma_x^2}{\sigma_n^2}. \tag{2.35}$$

The improvement of Γ with respect to Γ_{AWGN}, defined in (2.4), is given by

$$\gamma = \Gamma/\Gamma_{AWGN} = \left|\mathbf{u}_{BB}^H \mathbf{U}_{RF}^H \mathbf{H}\mathbf{F}_{RF}\mathbf{f}_{BB}\right|^2 \tag{2.36}$$

Optimization problem

From (2.36) on designing the precoder/beamformer the maximization problem is

$$\begin{aligned} \underset{\mathbf{F}_{RF},\mathbf{f}_{BB},\mathbf{U}_{RF},\mathbf{u}_{BB}}{\arg\max} \quad & \left|\mathbf{u}_{BB}^{H}\mathbf{U}_{RF}^{H}\mathbf{H}\mathbf{F}_{RF}\mathbf{f}_{BB}\right|^{2} \\ with \quad & \left|[\mathbf{F}_{RF}]_{i,j}\right| = 1, \quad i = 1,...,M, \quad j = 1,...,M_{RF} \\ & \left|[\mathbf{U}_{RF}]_{i,j}\right| = 1, \quad i = 1,...,N, \quad j = 1,...,N_{RF} \\ & ||\mathbf{F}_{RF}\mathbf{f}_{BB}||^{2} = 1 \\ & ||\mathbf{U}_{RF}\mathbf{u}_{BB}||^{2} = 1 \end{aligned} \tag{2.37}$$

where the constraints underline that the RF part of beamformer must apply changes only on signal phases, and, as usual, beamformers do not amplify power.

2.5.3 Precoder and combiner design

In [8] beamformers $\mathbf{F}_{RF}$ and $\mathbf{f}_{BB}$ are evaluated by the knowledge of vectors $\mathbf{a}_t$ in (1.4) as a solution to the following problem

$$\min_{\mathbf{F}_{RF},\mathbf{f}_{BB}} ||\boldsymbol{f}_{MRB} - \mathbf{F}_{RF}\mathbf{f}_{BB}||^{2} \tag{2.38a}$$

$$s.t. \quad col_j\left(\mathbf{F}_{RF}\right) \in \left\{\mathbf{a}_t\left(\phi_{\ell}^{(t)}\right), 1 \le \ell \le L\right\}, \; j = 1,...,M_{RF} \tag{2.38b}$$

$$with \quad ||\mathbf{F}_{RF}\mathbf{f}_{BB}||^{2} = 1 \tag{2.38c}$$

Similar procedure is used to evaluate $\mathbf{U}_{RF}$ and $\mathbf{u}_{BB}$ based on $\boldsymbol{u}_{MRB}$. In (2.38b) $col_j\left(\mathbf{F}_{RF}\right)$ denotes column j of matrix $\mathbf{F}_{RF}$. In other words, columns of $\mathbf{F}_{RF}$ are chosen among the L ray phase vector responses.
The problem in (2.38) consists of determining $\mathbf{F}_{RF}$ by selecting suitable columns of the following matrix

$$\mathbf{A}_t = \left[\mathbf{a}_t\left(\phi_1^{(t)}\right) \quad ... \quad \mathbf{a}_t\left(\phi_L^{(t)}\right)\right] \tag{2.39}$$

and corresponding evaluating $\mathbf{f}_{BB}$ by the least square (LS) method to solve (2.38a) under constraint (2.38c). This algorithm is reported in Tab. 2.1. The same algorithm can be used for determining $\mathbf{U}_{RF}$ and $\mathbf{u}_{BB}$ starting from $\boldsymbol{u}_{MRB}$ and $\mathbf{A}_r = \left[\mathbf{a}_r\left(\phi_1^{(r)}\right) \; ... \; \mathbf{a}_r\left(\phi_L^{(r)}\right)\right]$. If N_{RF} is different from M_{RF} better results are obtained by using an iterative procedure where transmit and receive beamformers are updated starting from $\boldsymbol{u}_{MRB} = \mathbf{H}\mathbf{F}_{RF}\mathbf{f}_{BB}$ when $M_{RF} < N_{RF}$ and $\boldsymbol{f}_{MRB} = \mathbf{H}^{H}\mathbf{U}_{RF}\mathbf{u}_{BB}$ when $M_{RF} > N_{RF}$. We just recall that functional (2.38a) requires as target the optimum composite beamformer $\boldsymbol{f}_{MRB}$.

Input:	$\boldsymbol{f}_{MRB}, \mathbf{A}_t$
1.	$\mathbf{F}_{RF} = 0$
2.	$\mathbf{f}_{BB} = 0$
3.	$\boldsymbol{f}_{res} = \boldsymbol{f}_{MRB}$
4.	**for** $i = 1$ **to** M_{RF}
5.	$\boldsymbol{\Psi} = \mathbf{A}_t^H \boldsymbol{f}_{res}$
6.	$o = \arg\max_{l \in 1,...,L} \left[\boldsymbol{\Psi}\boldsymbol{\Psi}^H\right]_{l,l}$
7.	$\mathbf{F}_{RF} = [\mathbf{F}_{RF} \vert col_o(\mathbf{A}_t)]$ (Add one column)
8.	$\mathbf{f}_{BB} = \left(\mathbf{F}_{RF}^H \mathbf{F}_{RF}\right)^{-1} \mathbf{F}_{RF}^H \boldsymbol{f}_{MRB}$
9.	$\boldsymbol{f}_{res} = \frac{\boldsymbol{f}_{MRB} - \mathbf{F}_{RF}\mathbf{f}_{BB}}{\|\boldsymbol{f}_{MRB} - \mathbf{F}_{RF}\mathbf{f}_{BB}\|}$
10.	**end for**
11.	$\mathbf{f}_{BB} = \frac{\mathbf{f}_{BB}}{\|\mathbf{F}_{RF}\mathbf{f}_{BB}\|}$

Table 2.1: ADB algorithm for the design of $\mathbf{F}_{RF}$ and $\mathbf{f}_{BB}$.

2.5.4 Performance results

Performance are, in terms of $\bar{\gamma}$, evaluated by averaging (2.36) for 5000 realizations of the channel. For a comparison we also report the MRB bound. Fig. 2.7 shows the average SNR improvement $\bar{\gamma}$ versus the number of antennas (number of Rx and Tx antennas is equal, i.e. $M = N$) for the ADB algorithm with $M_{RF} = N_{RF}$. We can see that performance of this algorithm are close to the bound.

2.6 Iterative Analog-digital beamforming (I-ADB)

The ADB algorithm, to design the analog and digital parts of precoder/beamformer, is quite complex since it requires as target design the singular value decomposition (SVD) of the channel matrix $\mathbf{H}$ which can be quite large. Also it makes use of an iterative procedure for the design of analog parts. Here we propose a much simpler iterative-ADB (I-ADB) algorithm, which is an example of application of the method presented in [13]. Firstly, by extending the approach in [8], the analog precoder/beamformer is obtained by stacking $\mathbf{A}_t$ ($\mathbf{A}_r$), i.e.

$$\mathbf{F}_{RF} = [\mathbf{A}_t, \mathbf{A}_t, ..., \mathbf{A}_t]_{0:M_{RF}-1} \quad and \quad \mathbf{U}_{RF} = [\mathbf{A}_r, \mathbf{A}_r, ..., \mathbf{A}_r]_{0:N_{RF}-1} \tag{2.40}$$

Next, referring to the scheme in Fig. 2.6 we would design the digital precoder $\mathbf{f}_{BB}$ and beamformer $\mathbf{u}_{BB}$ by the I-MRB algorithm [13] applied to the "digital " channel matrix whose dimension is only $M_{RF} \times N_{RF}$

$$\mathbf{G} = \mathbf{U}_{RF}^H \mathbf{H} \mathbf{F}_{RF} \tag{2.41}$$

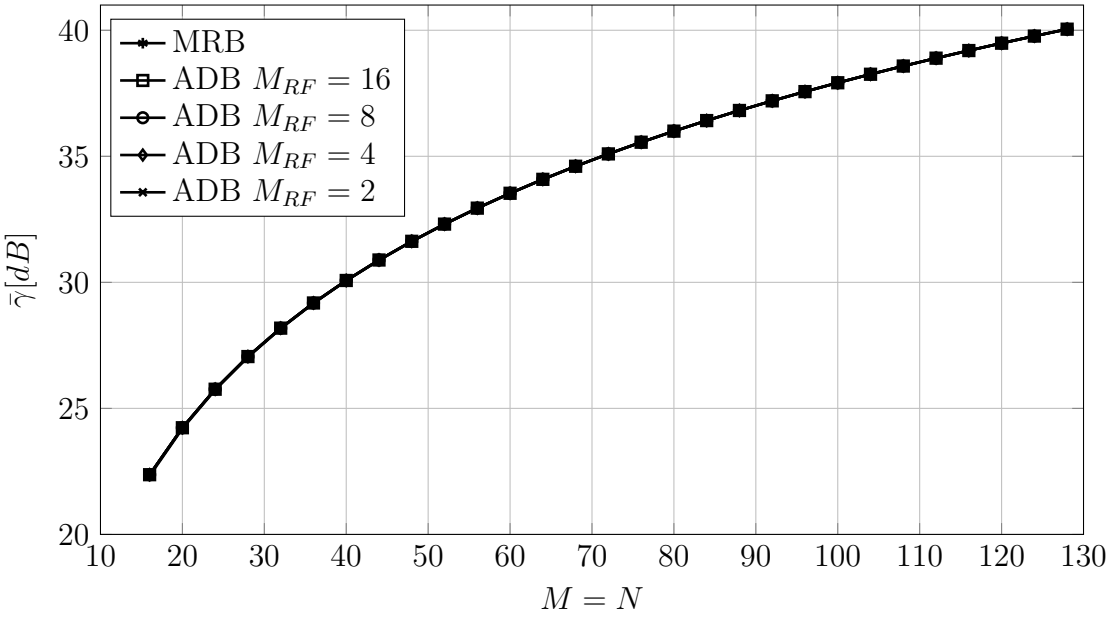

Figure 2.7: $\bar{\gamma}$ vs. M (and $M = N$) for the ADB algorithm with $M_{RF} = N_{RF}$.

In this case the optimization problem is

$$\max_{\mathbf{f}_{BB},\mathbf{u}_{BB}} |\mathbf{u}_{BB}^H \mathbf{G} \mathbf{f}_{BB}|^2 \tag{2.42a}$$

$$with \quad ||\mathbf{F}_{RF}\mathbf{f}_{BB}||^2 = 1, \quad ||\mathbf{U}_{RF}\mathbf{u}_{BB}||^2 = 1 \tag{2.42b}$$

and the iterative solution, exposed in Table 2.2, requires N_I iterations.

2.6.1 Performance results

Performance are, in terms of $\bar{\gamma}$, evaluated by averaging (2.36) for 5000 realizations of the channel. For a comparison we also report the MRB bound. Fig. 2.8 shows the average SNR improvement $\bar{\gamma}$ versus the number of antennas (number of Rx and Tx antennas is equal, i.e. $M = N$) for the I-ADB algorithm with $M_{RF} = N_{RF}$. We can see that performance using the I-ADB algorithm are close to the bound, especially for $M_{RF} = N_{RF} > 4$.
For completeness in the Appendix A we report the computational complexity of ADB and I-ADB algorithms. In Fig. 2.9, for $M_{RF} = N_{RF} = 8, 16$ and $N_I = 7$, we report the computational complexity of the two algorithms vs. $M = N$. We can see that the I-ADB complexity is lower than that of ADB.

Input:	$\mathbf{H}, \mathbf{F}_{RF}, \mathbf{U}_{RF}$
1.	$\mathbf{G} = \mathbf{U}_{RF}^H \mathbf{H} \mathbf{F}_{RF}$
2.	$\mathbf{u}_{BB} = \frac{1}{\sqrt{N_{RF}}}[1, 1, ..., 1]^T$
3.	**for** $i = 1$ **to** N_I
4.	$\mathbf{h}_{MISO} = \mathbf{u}_{BB}^H \mathbf{G}$
5.	$\mathbf{f}_{BB} = \frac{\mathbf{h}_{MISO}^H}{\|\mathbf{h}_{MISO}\|}$
6.	$\mathbf{h}_{SIMO} = \mathbf{G}\mathbf{f}_{BB}$
7.	$\mathbf{u}_{BB} = \frac{\mathbf{h}_{SIMO}}{\|\mathbf{h}_{SIMO}\|}$
8.	**end for**
9.	$\mathbf{f}_{BB} = \frac{\mathbf{f}_{BB}}{\|\mathbf{F}_{RF}\mathbf{f}_{BB}\|}$
10.	$\mathbf{u}_{BB} = \frac{\mathbf{u}_{BB}}{\|\mathbf{U}_{RF}\mathbf{u}_{BB}\|}$

Table 2.2: I-ADB algorithm for the design of $\mathbf{f}_{BB}$ and $\mathbf{u}_{BB}$.

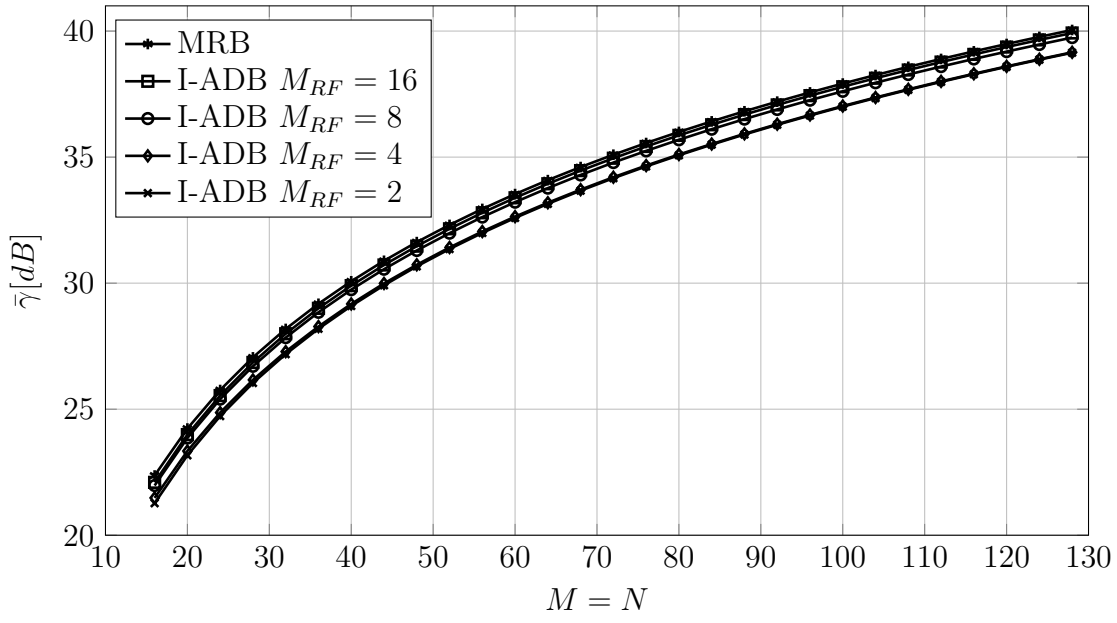

Figure 2.8: $\bar{\gamma}$ vs. M (and $M = N$) for the I-ADB algorithm with $M_{RF} = N_{RF}$.

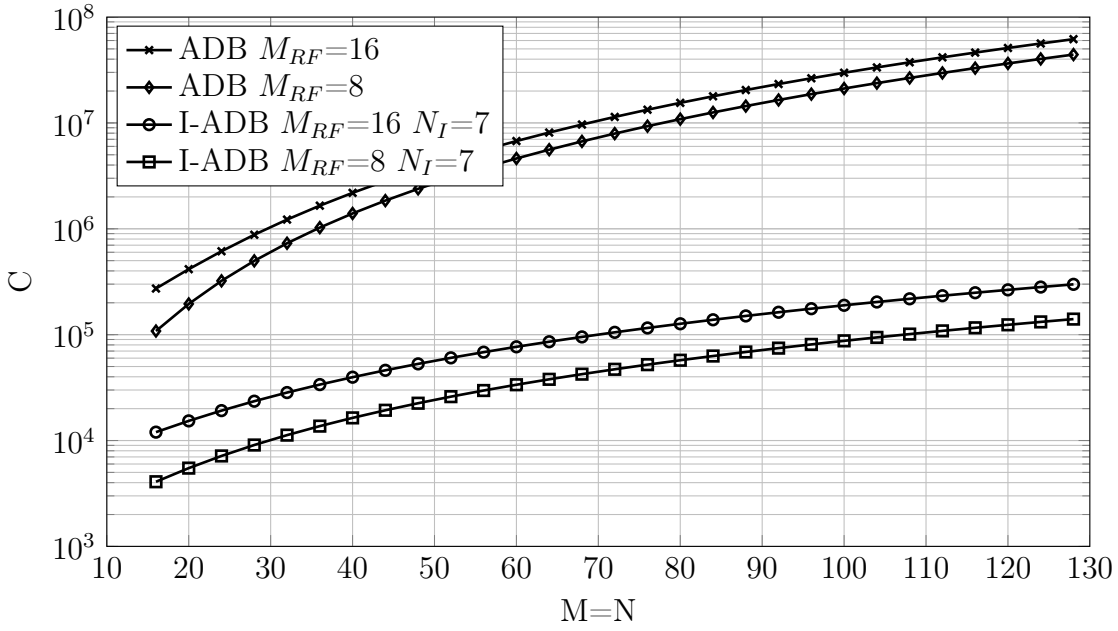

Figure 2.9: Computational complexity of ADB and I-ADB algorithms vs M (and $M = N$) with $M_{RF} = N_{RF}$.

Chapter 3

Vector quantized analog beamformers

In the previous section we described optimal and sub-optimal architectures. We have seen that in order to to design $\mathbf{f}_{BB}$, $\mathbf{u}_{BB}$, $\mathbf{F}_{RF}$ and $\mathbf{U}_{RF}$ ADB and I-ADB need to have knowledge of matrices $\mathbf{A}_t$ and $\mathbf{A}_r$, that are factors of the channel $\mathbf{H}$. To overcome this problem, we propose to choose matrices $\mathbf{F}_{RF}$ and $\mathbf{U}_{RF}$ in a dictionary and then calculate $\mathbf{f}_{BB}$ and $\mathbf{u}_{BB}$.

3.1 Vector quantization

Vector quantization (VQ) is introduced as a natural extension of the scalar quantization (SQ) concept. However, using multidimensional signals opens the way to many techniques and applications that are not found in the scalar case [16], [17]. The basic concept is that of associating with an input vector $\mathbf{s} = [1, ..., s_N]^T$, generic sample of a vector random process $\mathbf{s}(k)$, a reproduction vector $\mathbf{s} = \mathbf{Q}\mathbf{s}]$ chosen from a finite set of L elements (code vectors), $\mathcal{A} = \{\mathbf{Q}_1, ..., \mathbf{Q}_L\}$, called codebook, so that a given distortion measure $d(\mathbf{s}, \mathbf{Q}[\mathbf{s}])$ is minimized.

3.1.1 Characterization of VQ

Considering the general case of complex-valued signals, a vector quantizer is characterized by

- Input vector or matrix $\mathbf{s} = \begin{bmatrix} s_{1,1} & \dots & s_{1,M} \\ \vdots & \ddots & \vdots \\ s_{N,1} & \dots & s_{N,M} \end{bmatrix} \in \mathbb{C}^{N \times M}$
- Codebook $\mathcal{A} = \{\mathbf{Q}_i\}$, $i = 1, ..., L$ where $\mathbf{Q}_i \in \mathbb{C}^{N \times M}$ is a code vector.

- Distortion measure $d(\mathbf{s}, \mathbf{Q}_i)$.
- Quantization rule (minimum distortion)

$$\mathbf{Q} : \mathbb{C}^{N\times M} \to \mathcal{A} \quad with \quad \mathbf{Q}_i = \mathbf{Q}[\mathbf{s}] \quad if \quad i = \arg\min_{\ell} d(\mathbf{s}, \mathbf{Q}_\ell) \tag{3.1}$$

- Voronoi regions

$$R_\ell = \left\{\mathbf{s} \in \mathbb{C}^{N\times M} : \mathbf{Q}[\mathbf{s}] = \mathbf{Q}_\ell\right\} \quad \ell = 1, ..., L \tag{3.2}$$

3.1.2 LBG algorithm

To generate the codebook the LBG (Linde, Buzo, and Gray) algorithm [18] make use of very long realizations. The sequence used to design the VQ is called training sequence (TS) and is composed of K matrices/vectors.

$$\mathbf{s}(k), \quad k = 1, ..., K \tag{3.3}$$

The average distortion is now given by

$$D = \frac{1}{K}\sum_{k=1}^{K} d(\mathbf{s}(k), \mathbf{Q}[\mathbf{s}(k)]) \tag{3.4}$$

and the two rules to minimize D become:
Rule A

$$R_i = \{\mathbf{s}(k) : d(\mathbf{s}(k), \mathbf{Q}_i)\} = \min_{\mathbf{Q}_\ell \in \mathcal{A}} d(\mathbf{s}(k), \mathbf{Q}_\ell) \quad i = 1, ..., L \tag{3.5}$$

that is R_i is given by all the elements $\{\mathbf{s}(k)\}$ of the TS nearest to $\mathbf{Q}_i$.
Rule B

$$\mathbf{Q}_i = \arg\min_{\mathbf{Q}_j \in \mathbb{C}^{N\times M}} \frac{1}{m_i} \sum_{\mathbf{s}(k)\in R_i} d(\mathbf{s}(k), \mathbf{Q}_j) \tag{3.6}$$

where m_i is the number of elements of the TS that are inside R_i.

3.1.3 Description of the LBG algorithm with splitting procedure

The iterative algorithm start with a codebook with a number of elements $L = 1$. By slightly changing the components of this code vector (splitting procedure), we derive two code vectors and an initial alphabet with $L = 2$; at this point, using the LBG algorithm, we determine the optimum VQ for $L = 2$. At convergence, each optimum code vector is changed to obtain two new code vectors and the LBG algorithm is used

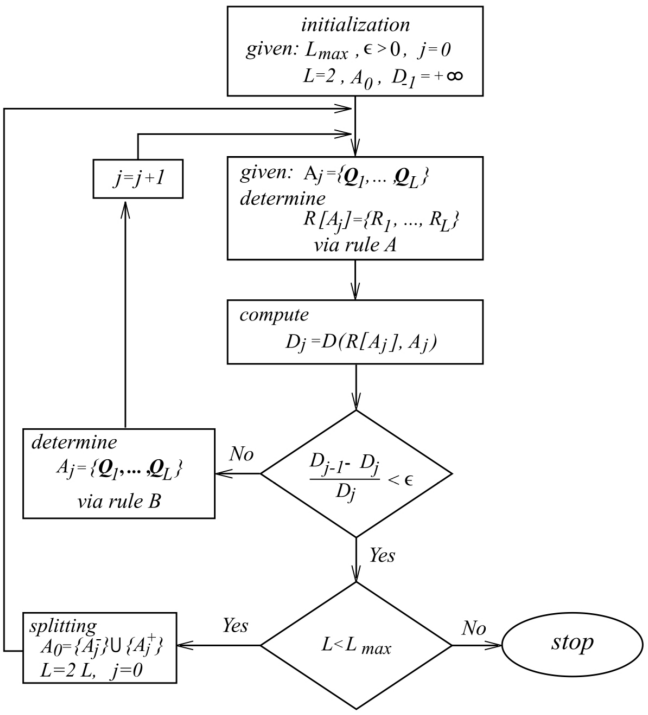

Figure 3.1: LBG algorithm with splitting procedure..

for $L = 4$. Iteratively the splitting procedure and optimization is repeated until the desired number of elements for the codebook is obtained. Let $\mathcal{A}_j = \{\mathbf{Q}_1, ..., \mathbf{Q}_L\}$ be the codebook at iteration j-th. The splitting procedure generates $2L$ N-dimensional vectors yielding the new codebook

$$\mathcal{A}_{j+1} = \{\mathcal{A}_j^-\} \cup \{\mathcal{A}_j^+\} \tag{3.7}$$

where

$$\mathcal{A}_j^- = \{\mathbf{Q}_i - \boldsymbol{\epsilon}_-\} \quad i = 1, ..., L \tag{3.8}$$
$$\mathcal{A}_j^+ = \{\mathbf{Q}_i - \boldsymbol{\epsilon}_+\} \quad i = 1, ..., L \tag{3.9}$$
$$\tag{3.10}$$

Typically $\boldsymbol{\epsilon}_-$ is the zero vector,

$$\boldsymbol{\epsilon}_- = \mathbf{0} \tag{3.11}$$

and

$$\boldsymbol{\epsilon}_+ = \frac{1}{10}\sqrt{\frac{M_s}{N}} \cdot \mathbf{1} \tag{3.12}$$

Choosing $\epsilon > 0$ (typically $\epsilon = 10^{-3}$) and an initial alphabet given by the splitting procedure applied to the average of the TS, we obtain the LBG algorithm, whose block diagram is shown in Figure 3.1.

3.2 Codebook design

To overcome the knowledge of $\mathbf{A}_t$ ($\mathbf{A}_r$) (2.39), which may be quite hard to obtain (see [9]), we choose $\mathbf{F}_{RF}$ ($\mathbf{U}_{RF}$) between the elements of a dictionary and then calculate $\mathbf{f}_{BB}$ ($\mathbf{u}_{BB}$) by the LS method.
The problem is finding, through the LBG algorithm [23], a codebook for $\mathbf{F}_{RF}$ ($\mathbf{U}_{RF}$). Offline, for each of 5000 channel matrix realizations (training sequence), we evaluate $\mathbf{F}_{RF}$ ($\mathbf{U}_{RF}$) by the ADB algorithm. Next we run the LBG algorithm to obtain the codebook $\mathcal{D}_{TX}$ ($\mathcal{D}_{RX}$) of size L_{TX} (L_{RX}) using as metric the phase-invariant distance between any two matrices $\mathbf{F}$ and $\mathbf{Q}$ defined as

$$d(\mathbf{F}, \mathbf{Q}) = \sqrt{2\left(1 - |\mathbf{v}_F^H \mathbf{v}_Q|\right)} \tag{3.13}$$

where $\mathbf{v}_F = vec(\mathbf{F})$, $\mathbf{v}_Q = vec(\mathbf{Q})$, $||\mathbf{F}|| = ||\mathbf{Q}|| = 1$, if $vec(\mathbf{F})$ is the vectorization of matrix $\mathbf{F}$. If $\mathbf{F}$ denotes a matrix of the training sequence and $\mathbf{Q}$ a quantized codeword, to ensure the unitary magnitude of each element of $\mathbf{Q}$, in every step of the LBG algorithm we normalize the elements of the matrices obtained. From the codebooks

$$\mathcal{D}_{TX} = \left\{\mathbf{Q}_{TX,1}, ..., \mathbf{Q}_{TX,L_{TX}}\right\}, \quad \mathcal{D}_{RX} = \left\{\mathbf{Q}_{RX,1}, ..., \mathbf{Q}_{RX,L_{RX}}\right\}, \tag{3.14}$$

we calculate for every codeword the pseudoinverse matrix

$$\mathbf{Q}_{TX,i}^{PI} = \left(\mathbf{Q}_{TX,i}^H \mathbf{Q}_{TX,i}\right)^{-1} \mathbf{Q}_{TX,i}^H, \quad \mathbf{Q}_{RX,i}^{PI} = \left(\mathbf{Q}_{RX,i}^H \mathbf{Q}_{RX,i}\right)^{-1} \mathbf{Q}_{RX,i}^H. \tag{3.15}$$

3.3 Quantized analog digital beamforming (Q-ADB)

We simply replace $\mathbf{F}_{RF}$ in the ADB algorithm with a codeword of the codebook. Hence in (2.38a) we range across all codewords to find the best one. In other words we define the new functionals:

$$\begin{gathered} \min_{\mathbf{F}_{RF} \in \mathcal{D}_{TX}, \mathbf{f}_{BB}} ||\boldsymbol{f}_{MRB} - \mathbf{F}_{RF}\mathbf{f}_{BB}||^2 \\ with \quad ||\mathbf{F}_{RF}\mathbf{f}_{BB}||^2 = 1 \end{gathered} \tag{3.16}$$

and

$$\begin{gathered} \min_{\mathbf{U}_{RF} \in \mathcal{D}_{RX}, \mathbf{u}_{BB}} ||\boldsymbol{u}_{MRB} - \mathbf{U}_{RF}\mathbf{u}_{BB}||^2 \\ with \quad ||\mathbf{U}_{RF}\mathbf{u}_{BB}||^2 = 1 \end{gathered} \tag{3.17}$$

Input:	$\boldsymbol{f}_{MRB}, \mathcal{D}_{TX}$
1.	$J_{TX} = +\infty$
2.	**for** $i = 1$ **to** L_{TX}
3.	$\quad \mathbf{f}_{temp} = \mathbf{Q}_{TX,i}^{PI} \boldsymbol{f}_{MRB}$
4.	$\quad J_{temp} = \|\|\boldsymbol{f}_{MRB} - \mathbf{Q}_{TX,i}\mathbf{f}_{temp}\|\|^2$
5.	$\quad$ **if** $J_{temp} < J_{TX}$
6.	$\quad\quad \mathbf{F}_{RF} = \mathbf{Q}_{TX,i}$
7.	$\quad\quad \mathbf{f}_{BB} = \mathbf{f}_{temp}$
8.	$\quad\quad \mathbf{J}_{TX} = \mathbf{J}_{temp}$
9.	$\quad$ **end if**
10.	**end for**
11.	$\mathbf{f}_{BB} = \frac{\mathbf{f}_{BB}}{\|\|\mathbf{F}_{RF}\mathbf{f}_{BB}\|\|}$

Table 3.1: Q-ADB algorithm for the design of $\mathbf{F}_{RF}$ and $\mathbf{f}_{BB}$.

To solve (3.16) we propose the exhaustive algorithm shown in Tab. 3.1. We can use the same algorithm to solve (3.17). As for the ADB algorithm, an iterative procedure can be used for determining iterativly $\mathbf{U}_{RF}$ and $\mathbf{u}_{BB}$ given $\mathbf{F}_{RF}$ and $\mathbf{f}_{BB}$ and vice versa. We just note that also the Q-ADB algorithm requires $\boldsymbol{f}_{MRB}$.

3.3.1 Performance results

Performance, in terms of $\bar{\gamma}$, are evaluated by averaging (2.36) for the same 5000 realizations of the channel. Obviously these realizations are different from the ones used in the vector quantization.
Fig. 3.2 shows the average SNR improvement $\bar{\gamma}$ versus the number of antennas (number of Rx and Tx antennas is equal, i.e. $M = N$) for the Q-ADB algorithm for four values of the codebook size and two values of the number of RF chains. For a comparison we also report the MRB bound. We recall that the ADB algorithm yields the same performance of the bound. We note that although the Q-ADB yields lower performance than ADB, they improve if we use more RF chains and an higher codebook size. For 16 RF chains and a codebook size of 64 for $M = N = 16$ performance are very close to the bound. However if $M = N$ is increased performance saturate due to the vector quantization limited representation.

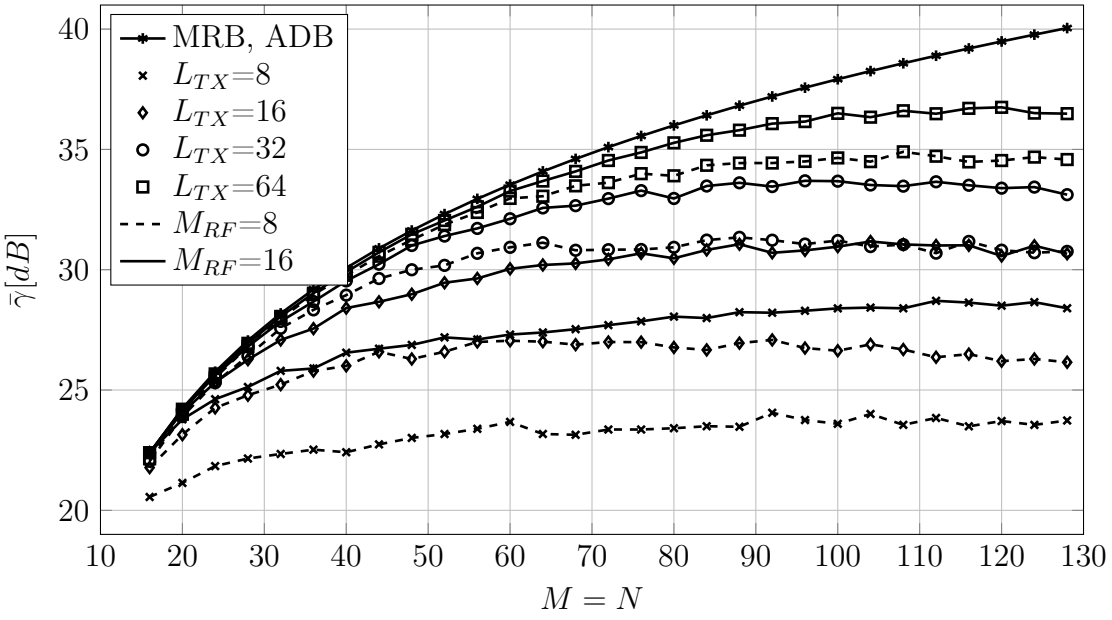

Figure 3.2: $\bar{\gamma}$ vs M (and $M = N$) for the Q-ADB algorithm using different codebook sizes ($L_{TX} = L_{RX}$) and two values of $M_{RF} = N_{RF}$.

3.4 Quantized iterative analog digital beamforming (QI-ADB)

This method does not make use of $\boldsymbol{f}_{MRB}$. In fact, referring to the scheme in Fig. 2.6 we would design the base band beamformers $\mathbf{f}_{BB}$ and $\mathbf{u}_{BB}$ by the I-MRB algorithm [13] applied to the "digital " channel matrix whose dimension is only $M_{RF} \times N_{RF}$

$$\begin{aligned} \mathbf{G} &= \mathbf{U}_{RF}^H \mathbf{H} \mathbf{F}_{RF} \\ with \quad & \mathbf{F}_{RF} \in \mathcal{D}_{TX}, \quad \mathbf{U}_{RF} \in \mathcal{D}_{RX} \end{aligned} \tag{3.18}$$

We recall that the I-MRB algorithm consists in a simple approach which alternatively makes use of a multi input single output (MISO) and single input multiple output (SIMO) configuration and converges in a small number of iteration N_I to the MRB solution, in the case of full digital beamformers. In our case, the functional is now (2.36), hence in formula the problem is

$$\max_{\mathbf{F}_{RF} \in \mathcal{D}_{TX}, \mathbf{f}, \mathbf{U}_{RF} \in \mathcal{D}_{RX}, \mathbf{u}} |\mathbf{u}^H \mathbf{G} \mathbf{f}|^2 \tag{3.19a}$$

$$with \quad ||\mathbf{F}_{RF} \mathbf{f}_{BB}||^2 = 1, \quad ||\mathbf{U}_{RF} \mathbf{u}_{BB}||^2 = 1 \tag{3.19b}$$

To solve the problem (3.19), we propose the exhaustive algorithm shown in Tab. 3.2.

Input:	$\mathcal{D}_{TX}, \mathcal{D}_{RX}, \mathbf{G}$
1.	$\gamma = 0$
2.	**for** $i = 1$ **to** L_{Tx}
3.	**for** $j = 1$ **to** L_{Rx}
4.	$\mathbf{G} = \mathbf{Q}_{Tx,i}^{H} \mathbf{H} \mathbf{Q}_{Rx,j}$
5.	$(\mathbf{f}_{temp}, \mathbf{u}_{temp}) = IMRB(\mathbf{G}, N_I)$
6.	$\mathbf{f}_{temp} = \frac{\mathbf{f}_{temp}}{\|\|\mathbf{Q}_{Tx,i}\mathbf{f}_{temp}\|\|}$
7.	$\mathbf{u}_{temp} = \frac{\mathbf{u}_{temp}}{\|\|\mathbf{Q}_{Rx,i}\mathbf{u}_{temp}\|\|}$
8.	$\gamma_{temp} = \|\mathbf{u}_{temp}^{H} \mathbf{G} \mathbf{f}_{temp}\|^2$
9.	**if** $\gamma_{temp} > \gamma$
10.	$\gamma = \gamma_{temp}$
11.	$\mathbf{F}_{RF} = \mathbf{Q}_{Tx,i}; \quad \mathbf{f}_{BB} = \mathbf{f}_{temp}$
12.	$\mathbf{U}_{RF} = \mathbf{Q}_{Rx,j}; \quad \mathbf{u}_{BB} = \mathbf{u}_{temp}$
13.	**end if**
14.	**end for**
15.	**end for**

Table 3.2: QI-ADB algorithm for the design of $\mathbf{F}_{RF}$, $\mathbf{f}_{BB}$, $\mathbf{U}_{RF}$ and $\mathbf{u}_{BB}$.

We should to note that the QI-ADB algorithm may yield a sub-optimal solution, as the iterative design procedure may not converge to the optimal solution, mainly because it does not make use of a target for the beamformers, unlike the Q-ADB that makes use of $\boldsymbol{f}_{MRB}$ and $\boldsymbol{u}_{MRB}$.

3.4.1 Performance results

As for ADB algorithm performance are, in terms of $\bar{\gamma}$, evaluated by averaging (2.36) for the same 5000 realizations of the channel. Obviously these realizations are different from the ones used in the vector quantization.
In Fig. 3.3 we report $\bar{\gamma}$ for the QI-ADB algorithm, with a number of iteration $N_I = 7$. We can see that for a small number of RF chains, for example $M_{RF} = 4$, $\bar{\gamma}$ is equal or even better than for systems with a greater number of RF chains. In fact we expected performance to increase for higher values of M_{RF}, as the digital beamformers become more effective. However, this happens only if vector quantization adequately represents the analog beamformer, i.e. if L_{TX} (L_{RX}) is sufficiently high. Moreover if the codebook size is small and also M_{RF} is small (i.e. large analog beamformers), vector quantization may not represent the analog beamformers adequately and performance are erratic. Also in this algorithm, for a given L_{TX} and M_{RF}, after a certain value of $M = N$, $\bar{\gamma}$ saturates.

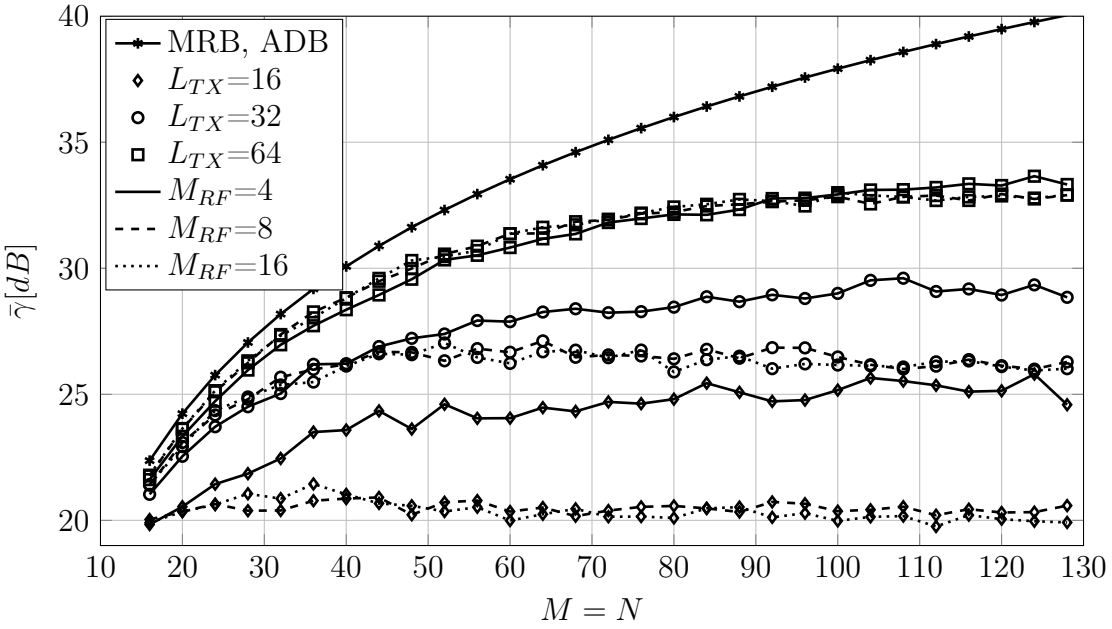

Figure 3.3: $\bar{\gamma}$ vs M (and $M = N$) for the QI-ADB algorithm using different codebook sizes ($L_{TX} = L_{RX}$) and three values of $M_{RF} = N_{RF}$.

Now we compare the two proposed algorithms. We set a target of $\bar{\gamma}$ equal to $31dB$ for a system with $M = N = 64$ antennas. It is seen that Q-ADB and QI-ADB algorithms yield similar performance for the following parameter values: for the Q-ADB we need $M_{RF} = N_{RF} = 16$ and $L_{TX} = L_{RX} = 32$, while for the QI-ADB it is $M_{RF} = N_{RF} = 4$ and $L_{TX} = L_{RX} = 64$. In general, for the same performance, QI-ADB suffers a penalty of a greater codebook size with respect to Q-ADB.
For completeness in the Appendix we report the computational complexity of these algorithms. In Fig. 3.4, for the parameter values that yield similar performance of Q-ADB and QI-ADB, we report the computational complexity of the four algorithms vs. $M = N$. We can see that the computation complexity of the quantized algorithms and ADB is similar if M (and $N = M$) is greater than 120. In general for the parameter values of interest complexity of Q-ADB is similar to that of ADB, which however needs to know the channel structure, in particular the ray phase vector responses (1.3).

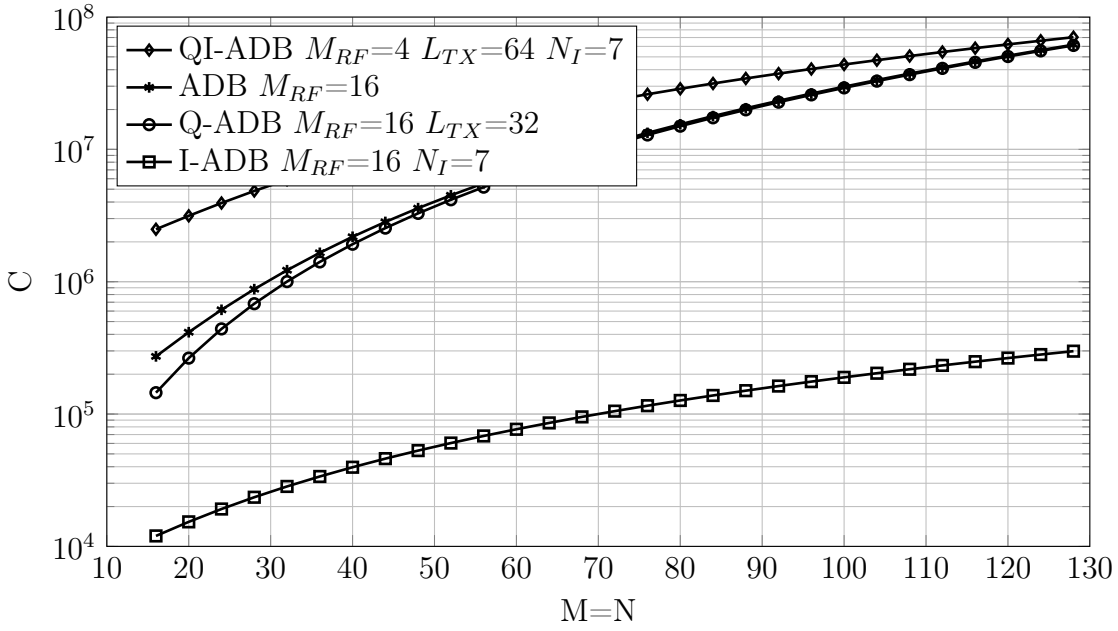

Figure 3.4: Computational complexity of four algorithms (ADB, I-ADB, Q-ADB, QI-ADB) vs M (and $M = N$) with $M_{RF} = N_{RF}$ and $L_{TX} = L_{RX}$.

Chapter 4

Channel estimation

In this chapter, based on a realistic finite ray channel model which captures both the limited scattering at high frequency and the antenna correlation of large arrays [19], we focus on channel estimation, which plays a key role for the hybrid precoder/beamformer design. We develop a specific training sequence of precoders and beamformers in order to estimate the channel parameters. Once these parameters are estimated, we can i) reconstruct the elements of the channel matrix and ii) design the transmit precoder and receive beamformer using the I-ADB algorithm. We propose two different approaches to estimate channel, the first based on Discrete Fourier Transform (DFT), while the second based on two-dimensional DFT.

4.1 Channel estimation using DFT

4.1.1 Estimate of angles of arrival and channel gains

From (1.4), (2.33) can be rewritten as

$$\mathbf{y}_{BB} = \mathbf{U}_{RF}^{H}\mathbf{y}_{RF} \tag{4.1}$$

with

$$\mathbf{y}_{RF} = \frac{1}{\sqrt{L}}\mathbf{A}_r\mathbf{H}_g\mathbf{A}_t^{H}\mathbf{x}_{RF} + \mathbf{n} \tag{4.2}$$

To estimate the angles of arrival $\phi_\ell^{(r)}$ and the channel gains g_ℓ we turn on only the first transmit antenna and turn off the others $M-1$. The same results is obtained by switching on all transmit antennas, and setting

$$\mathbf{x}_{BB} = \frac{1}{M_{RF}}\begin{bmatrix}1 & 1 & \dots & 1\end{bmatrix}^T \tag{4.3}$$

and

$$\mathbf{F}_{RF} = \begin{bmatrix} 1 & 1 & 1 & \dots & 1 \\ 1 & -1 & 1 & \dots & -1 \\ 1 & -1 & 1 & \dots & -1 \\ \vdots & \vdots & \vdots & \ddots & \vdots \\ 1 & -1 & 1 & \dots & -1 \end{bmatrix} \tag{4.4}$$

under the assumption M_{RF} is even, where the first row is of all 1's while the other rows contain the sequence (1,-1) repeated. In any case we get

$$\mathbf{x}_{RF} = \begin{bmatrix} 1 & 0 & \dots & 0 \end{bmatrix}^T \tag{4.5}$$

For this input to the system, the RF signal at the receiver (4.2) becomes

$$\begin{aligned} \mathbf{y}_{RF} &= \frac{1}{\sqrt{L}} \mathbf{A}_r \begin{bmatrix} g_1 \\ g_2 \\ \vdots \\ g_L \end{bmatrix} + \mathbf{n} \\ &= \frac{1}{\sqrt{L}} \begin{bmatrix} g_1 + ... + g_L \\ g_1 e^{j\zeta D \sin\left(\phi_1^{(r)}\right)} + ... + g_L e^{j\zeta D \sin\left(\phi_L^{(r)}\right)} \\ \vdots \\ g_1 e^{j\zeta D(N-1) \sin\left(\phi_1^{(r)}\right)} + ... + g_L e^{j\zeta D(N-1) \sin\left(\phi_L^{(r)}\right)} \end{bmatrix} + \mathbf{n} \end{aligned} \tag{4.6}$$

Unfortunately we only have access to $\mathbf{y}_{BB}$ as in (4.1). Let N_D be an integer, with $N_D \leq N$, a suitable parameter to be chosen. In order to derive $\mathbf{y}_{RF}$ as given by (4.6) we apply the following procedure at the receiver which makes use of $N_S = \left\lceil \frac{N_D}{N_{RF}} \right\rceil$ $\mathbf{U}_{RF}$ matrices of the form

$$\mathbf{U}_{RF}^{(s)} = \begin{bmatrix} \mathbf{0} \\ \vdots \\ \mathbf{0} \\ \bar{\mathbf{U}}_{RF} \\ \mathbf{0} \\ \vdots \\ \mathbf{0} \end{bmatrix} \begin{matrix} \Big\} sN_{RF} \\ \\ \\ \\ \Big\} N - (s+1)N_{RF} \end{matrix} \qquad s = 0, 1, ..., N_S - 1 \tag{4.7}$$

where $\bar{\mathbf{U}}_{RF}$ is a $N_{RF} \times N_{RF}$ square matrix, whose elements are chosen at random with unitary magnitude and such that $\bar{\mathbf{U}}_{RF}$ has full rank (see also Appendix B). Note that $\mathbf{U}_{RF}^{(s)}$ in (4.7) corresponds to switching on at the receiver only antennas

$sN_{RF}, ..., (s+1)N_{RF}-1$. Each $\mathbf{U}_{RF}^{(s)}$ will yield a corresponding $\mathbf{y}_{BB}^{(s)}$. Moreover if $\bar{\mathbf{U}}_{RF}$ has full rank, from (4.1) we get

$$[\mathbf{y}_{RF}]_{sN_{RF}:(s+1)N_{RF}-1} = (\bar{\mathbf{U}}_{RF}^{H})^{-1}\mathbf{y}_{BB}^{(s)}, \quad s = 0, 1, ..., N_S - 1 \tag{4.8}$$

Stacking all column vectors (4.8) in a single vector, we have

$$[\mathbf{y}_{RF}]_{0:N_D-1} = \frac{1}{\sqrt{L}} \begin{bmatrix} g_1 + ... + g_L \\ g_1 e^{j\zeta D \sin\left(\phi_1^{(r)}\right)} + ... g_L e^{j\zeta D \sin\left(\phi_L^{(r)}\right)} \\ \vdots \\ g_1 e^{j\zeta D(N_D-1) \sin\left(\phi_1^{(r)}\right)} + ... + g_L e^{j\zeta D(N_D-1) \sin\left(\phi_L^{(r)}\right)} \end{bmatrix} + [\mathbf{n}]_{0:N_D-1} \tag{4.9}$$

which is similar to (4.6) with N replaced by N_D. Let

$$\theta_\ell^{(r)} = \zeta D \sin\left(\phi_\ell^{(r)}\right) \tag{4.10}$$

the n-th element of $\mathbf{y}_{RF}$ in (4.9) can be written as

$$y_n = [\mathbf{y}_{RF}]_n = \frac{1}{\sqrt{L}} \left(g_1 e^{jn\theta_1^{(r)}} + \ldots + g_L e^{jn\theta_L^{(r)}} \right) + [\mathbf{n}]_n, \quad n = 0, 1, ..., N_D - 1 \tag{4.11}$$

i.e. y_n is equal to the sum of L complex modes each of phase $\theta_\ell^{(r)}$ and amplitude g_ℓ. To find the $2L$ parameters of complex modes we can compute the DFT of y_n on N_{DFT} samples with $N_{DFT} \geq N_D$, setting $y_n = 0$ for $n > N_D - 1$. In fact the DFT of y_n, scaled by N_D, becomes

$$Y(k) = \frac{1}{N_D} \sum_{n=0}^{N_{DFT}-1} y_n e^{-j2\pi \frac{kn}{N_{DFT}}} = \frac{1}{N_D} \sum_{n=0}^{N_D-1} y_n e^{-j2\pi \frac{kn}{N_{DFT}}} \tag{4.12}$$

Let us define

$$d(n) = \begin{cases} 1/N_D, & n = 0, 1, ..., N_D - 1 \\ 0, & otherwise \end{cases} \tag{4.13}$$

with

$$D(k) = DFT\{d(n)\} = e^{-j\frac{2\pi k}{N_{DFT}} \frac{N_D-1}{2}} sinc_{N_D}\left(k \frac{N_D}{N_{DFT}}\right) \tag{4.14}$$

and $sinc_{N_D}(x) = \frac{\sin(\pi x)}{N_D \sin(\pi x / N_D)}$.
Assuming N_{DFT} is large enough that it always exists an integer k_ℓ that

$$\theta_\ell^{(r)} = 2\pi \frac{k_\ell}{N_{DFT}} \tag{4.15}$$

Input:	$Y(k)$
1.	$Y_1(k) = Y(k)$
2.	**for** $i = 1$ **to** L
3.	$\hat{k}_i = \arg\max_k \lvert Y_i(k)\rvert$
4.	$\hat{g}_i = Y_i(\hat{k}_i)\sqrt{L}$
5.	$Y_{i+1}(k) = Y_i(k) - \frac{1}{\sqrt{L}}\hat{g}_i D(k - \hat{k}_i)$
6.	**end for**

Table 4.1: Cancellation method to estimate the channel parameters.

from (4.11) we can write

$$Y(k) = \frac{1}{\sqrt{L}}\left[g_1 D(k-k_1) + \ldots + g_L D(k-k_L))\right] + N(k), \quad k = 0, 1, ..., N_{DFT} - 1 \tag{4.16}$$

with $N(k) \sim \mathcal{CN}\left(0, \frac{\sigma_n^2}{N_D}\right)$. From (4.16) we can apply the method outlined in Table 4.1 to estimate the parameters of different modes. In practice also the number of modes L should be estimated by stopping the cancellation method when $|\hat{g}_i|$ turns out much smaller than $|\hat{g}_1|$. Here we simply assume that L is known. Next, from estimate of $\hat{k}_\ell$, and using (4.10) and (4.15), we obtain

$$\hat{\phi}_\ell^{(r)} = sin^{-1}\left(\frac{2\pi\hat{k}_\ell}{\zeta D N_{DFT}}\right). \tag{4.17}$$

By this method we can estimate the angles of arrival $\phi_\ell^{(r)}$ and the channel gains g_ℓ. We should note that higher values of N_D yield an estimate with lower noise level. Moreover, increasing N_{DFT} in (4.15) allows a better accuracy in the estimate of $\phi_\ell^{(r)}$. Note that this approach which determines (4.9) by (4.8) needs a training sequence of

$$N_{TS}^{(r)} = \left\lceil \frac{N_D}{N_{RF}} \right\rceil \tag{4.18}$$

transmit symbols or time slots and at each transmit symbol a specific known analog precoder/beamformer is set. However no iterative exchange of information is required between receiver and transmitter.

4.1.2 Estimate of angles of departure and channel gains

To estimate the angles of departure $\phi_\ell^{(t)}$ and the coefficients g_ℓ we switch on only the first receive antenna hence it is like selecting

$$\mathbf{U}_{RF} = \begin{bmatrix} 1 & 1 & 1 & \dots & 1 \\ 0 & 0 & 0 & \dots & 0 \\ 0 & 0 & 0 & \dots & 0 \\ \vdots & \vdots & \vdots & \ddots & \vdots \\ 0 & 0 & 0 & \dots & 0 \end{bmatrix} \tag{4.19}$$

Defined $\theta_\ell^{(t)} = \zeta D \sin\left(\phi_\ell^{(t)}\right)$ (4.1) becomes

$$\mathbf{y}_{BB} = \frac{1}{\sqrt{L}} \begin{bmatrix} g_1 & \dots & g_L \\ g_1 & \dots & g_L \\ \vdots & \ddots & \vdots \\ g_1 & \dots & g_L \end{bmatrix} \begin{bmatrix} 1 & e^{-j\theta_1^{(t)}} & \dots & e^{-j(M-1)\theta_1^{(t)}} \\ 1 & e^{-j\theta_2^{(t)}} & \dots & e^{-j(M-1)\theta_2^{(t)}} \\ \vdots & \vdots & \ddots & \vdots \\ 1 & e^{-j\theta_L^{(t)}} & \dots & e^{-j(M-1)\theta_L^{(t)}} \end{bmatrix} \mathbf{x}_{RF} + [\mathbf{n}]_0 \begin{bmatrix} 1 \\ 1 \\ \vdots \\ 1 \end{bmatrix} \tag{4.20}$$

where the matrix with coefficients g_ℓ is $N_{RF} \times L$ while the matrix with complex modes is $L \times M$. At the transmission side we switch on only the first M_D transmit antennas and send a training sequence of symbols x of length M_D denoted by $(x)_m,\ m = 0, ..., M_D - 1$, which generates a sequence of $\mathbf{x}_{RF}^{(m)}$ signals of the form

$$\mathbf{x}_{RF}^{(m)} = [x_{RF,0}^{(m)}, x_{RF,1}^{(m)}, ..., x_{RF,M_D-1}^{(m)}, 0, ..., 0]^T \tag{4.21}$$

and corresponding $\mathbf{y}_{BB}^{(m)}$ whose first component is

$$[\mathbf{y}_{BB}^{(m)}]_0 = \frac{1}{\sqrt{L}}[g_1 ... g_L] \begin{bmatrix} 1 & e^{-j\theta_1^{(t)}} & \dots & e^{-j(M_D-1)\theta_1^{(t)}} \\ 1 & e^{-j\theta_2^{(t)}} & \dots & e^{-j(M_D-1)\theta_2^{(t)}} \\ \vdots & \vdots & \ddots & \vdots \\ 1 & e^{-j\theta_L^{(t)}} & \dots & e^{-j(M_D-1)\theta_L^{(t)}} \end{bmatrix} \bar{\mathbf{x}}_{RF}^{(m)} + [\mathbf{n}^{(m)}]_0 \tag{4.22}$$

where $\bar{\mathbf{x}}_{RF}^{(m)}$ denotes just the first M_D ($M_D \leq M$) components of $\mathbf{x}_{RF}^{(m)}$. Let

$$\bar{\boldsymbol{X}} = \begin{bmatrix} \bar{\mathbf{x}}_{RF}^{(0)} & \bar{\mathbf{x}}_{RF}^{(1)} & \dots & \bar{\mathbf{x}}_{RF}^{(M_D-1)} \end{bmatrix} \tag{4.23}$$

and $\bar{\mathbf{n}} = \begin{bmatrix} [\mathbf{n}^{(0)}]_0 & [\mathbf{n}^{(1)}]_0 & \dots & [\mathbf{n}^{(M_D-1)}]_0 \end{bmatrix}$ from (4.22) it is

$$\begin{bmatrix} [\mathbf{y}_{BB}^{(0)}]_0 \\ [\mathbf{y}_{BB}^{(1)}]_0 \\ \vdots \\ [\mathbf{y}_{BB}^{(M_D-1)}]_0 \end{bmatrix}^T = \frac{1}{\sqrt{L}}[g_1 ... g_L] \begin{bmatrix} 1 & e^{-j\theta_1^{(t)}} & \dots & e^{-j(M_D-1)\theta_1^{(t)}} \\ 1 & e^{-j\theta_2^{(t)}} & \dots & e^{-j(M_D-1)\theta_2^{(t)}} \\ \vdots & \vdots & \ddots & \vdots \\ 1 & e^{-j\theta_L^{(t)}} & \dots & e^{-j(M_D-1)\theta_L^{(t)}} \end{bmatrix} \bar{\boldsymbol{X}} + \bar{\mathbf{n}} \tag{4.24}$$

If $\bar{\boldsymbol{X}}$ has full rank we can right multiply (4.24) by $\bar{\boldsymbol{X}}^{-1}$ and obtain

$$\begin{bmatrix} y_0 \\ y_1 \\ \vdots \\ y_{M_D-1} \end{bmatrix} = \begin{bmatrix} [\mathbf{y}_{BB}^{(0)}]_0 \\ [\mathbf{y}_{BB}^{(1)}]_0 \\ \vdots \\ [\mathbf{y}_{BB}^{(M_D-1)}]_0 \end{bmatrix}^T \bar{\boldsymbol{X}}^{-1} = \frac{1}{\sqrt{L}} \begin{bmatrix} g_1 + ... + g_L \\ g_1 e^{-j\theta_1^{(t)}} + ... + g_L e^{-j\theta_L^{(t)}} \\ \vdots \\ g_1 e^{-j(M_D-1)\theta_1^{(t)}} + ... + g_L e^{-j(M_D-1)\theta_L^{(t)}} \end{bmatrix} + \tilde{\mathbf{n}} \tag{4.25}$$

with $\tilde{\mathbf{n}} = \bar{\mathbf{n}}\bar{\boldsymbol{X}}^{-1}$.

If $\bar{\mathbf{X}}$ is chosen as an Hadamard matrix [23] (see Appendix B) divided by $\sqrt{M_D}$, this guarantees the full rank of $\bar{\mathbf{X}}$, the unitary norm of $\mathbf{x}_{RF}^{(m)}$ and that $\tilde{\mathbf{n}}$ in (4.25) is still white. In fact as $\bar{\mathbf{X}}^T\bar{\mathbf{X}} = \mathbf{I}_{M_D}$ it is $\bar{\mathbf{X}}^{-1} = \bar{\mathbf{X}}^T$ and the noise autocorrelation matrix becomes

$$\mathbf{R}_{\tilde{\mathbf{n}}} = \left(\bar{\mathbf{X}}^{-1}\right)^T \mathbf{R}_{\bar{\mathbf{n}}}\bar{\mathbf{X}}^{-1} = \left(\bar{\mathbf{X}}^T\right)^T \sigma_n^2 \mathbf{I}_{M_D}\bar{\mathbf{X}}^T = \sigma_n^2 \bar{\mathbf{X}}\bar{\mathbf{X}}^T = \sigma_n^2 \mathbf{I}_{M_D} \tag{4.26}$$

In any case as the m-th element of (4.25) is of the form

$$y_m = \frac{1}{\sqrt{L}}\left(g_1 e^{-jm\theta_1^{(t)}} + ... + g_L e^{-jm\theta_L^{(t)}}\right) + [\tilde{\mathbf{n}}]_m \tag{4.27}$$

we can estimate parameters $\phi_\ell^{(t)}$ and g_ℓ of the L complex modes using the method of Table 4.1. Moreover we can average the new estimate of g_ℓ with that obtained in the previous section to obtain a more reliable estimate. Note that from (4.21) this procedure needs a training sequence of

$$N_{TS}^{(t)} = M_D \tag{4.28}$$

time slots. The total length of training sequence is

$$N_{TS} = N_{TS}^{(r)} + N_{TS}^{(t)} = \left\lceil \frac{N_D}{N_{RF}} \right\rceil + M_D \tag{4.29}$$

time slots.

4.1.3 Performance results

In this section, we present numerical results demonstrating the performance of the proposed channel estimate. Performance, in terms of $\bar{\gamma}$, are evaluated by averaging (2.36) for the same 5000 realizations of the channel. After estimate of the channel parameters, and reconstruction (1.4) of the channel from the parameters, we apply the I-ADB algorithm to design the analog and digital precoders/beamformers with

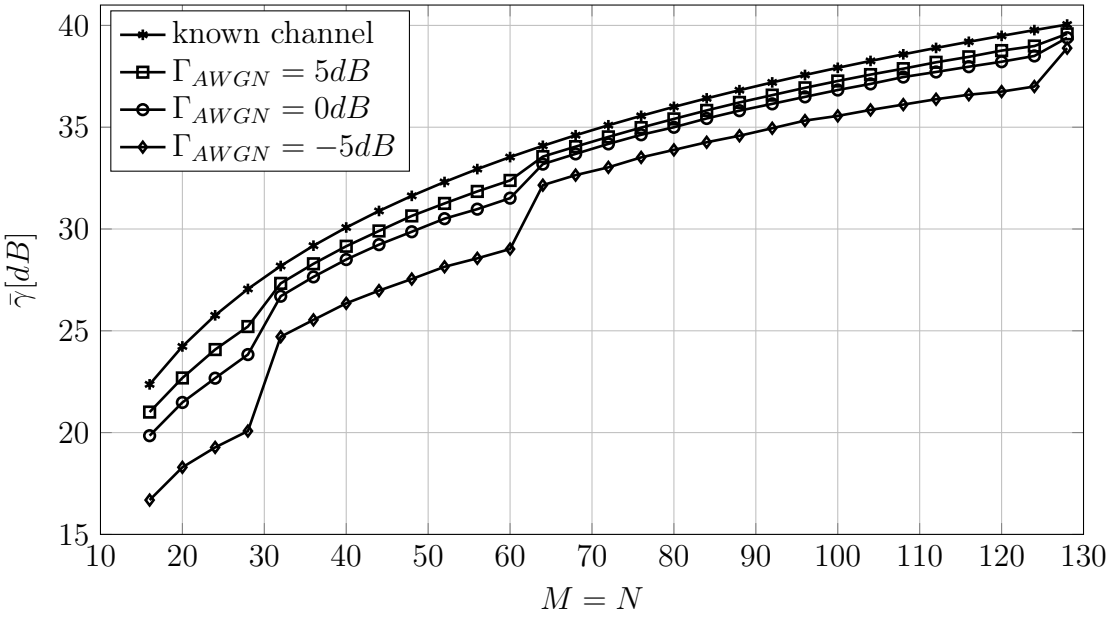

Figure 4.1: $\bar{\gamma}$ vs. M (and $M = N$) for the I-ADB algorithm in the presence of channel estimate with $M_D = N_D = 2^{\lfloor \log_2(M) \rfloor}$.

$N_I = 7$.
We show the average SNR improvement $\bar{\gamma}$ versus the number of antennas, using the I-ADB algorithm, with $M_{RF} = N_{RF} = 8$ and $N_{DFT} = 2048$, in the presence of the above channel estimate. Figures 4.1 and 4.2 show the average SNR improvement $\bar{\gamma}$ versus the number of antennas $M = N$ for two values of $N_D = M_D$ which dictate the length of the training sequence N_{TS} as from (4.18) and (4.28).
In Fig. 4.1 $N_D = M_D = 2^{\lfloor \log_2(M) \rfloor}$ and in Fig. 4.2 $N_D = M_D = \frac{2^{\lfloor \log_2(M) \rfloor}}{2}$. For a comparison we also report the performance bound by assuming perfect channel knowledge. When it is seen that $\bar{\gamma}$ is independent of the channel noise. We can see that performance using the channel estimate aren't perfectly close to the bound, especially when the noise level is high. This is due to the fact that this method doesn't estimate very well two angles when they are close together. However, overall this method yields very good performance and has a low computational complexity and most importantly doesn't need a feedback channel, which corresponds to a fast estimate.
In Fig. 4.3 we investigated the effect of N_{DFT} on the channel estimate. For this we report $\bar{\gamma}$ versus the number of antennas for four value of N_{DFT}, $\Gamma_{AWGN} = 5dB$ and $M_D = N_D = 2^{\lfloor \log_2(M) \rfloor}$. We can see that for an higher number of antennas also N_{DFT} must increase, corresponding to a better accuracy in the angle estimate, otherwise performance deteriorate.

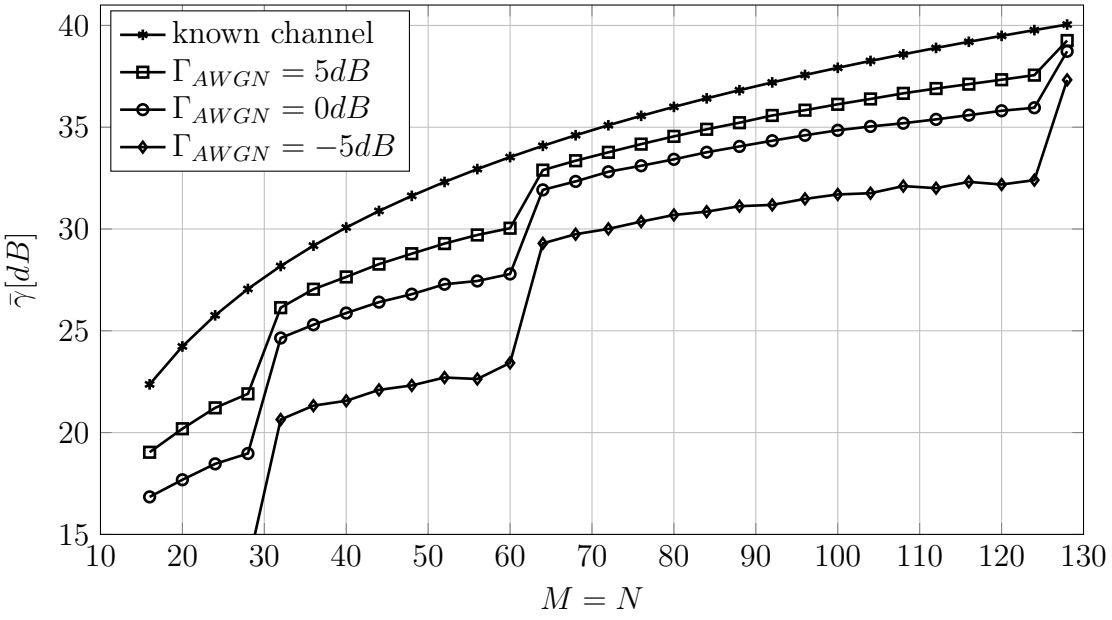

Figure 4.2: $\bar{\gamma}$ vs. M (and $M = N$) for the I-ADB algorithm in the presence of channel estimate with $M_D = N_D = \frac{2^{\lfloor \log_2(M) \rfloor}}{2}$.

4.2 Channel estimation using 2D-DFT

4.2.1 Estimate of channel parameters

From (1.4), set

$$\theta_\ell^{(t)} = \zeta D \sin\left(\phi_\ell^{(t)}\right), \quad \theta_\ell^{(r)} = \zeta D \sin\left(\phi_\ell^{(r)}\right) \tag{4.30}$$

element (n, m) of the channel matrix $\mathbf{H}$ can be written as

$$[\mathbf{H}]_{n,m} = \frac{1}{\sqrt{L}} \left(g_1 e^{jn\theta_1^{(r)}} e^{-jm\theta_1^{(t)}} + ... + g_\ell e^{jn\theta_\ell^{(r)}} e^{-jm\theta_\ell^{(t)}} + ... + g_L e^{jn\theta_L^{(r)}} e^{-jm\theta_L^{(t)}} \right) \tag{4.31}$$

with $n = 0, 1, ..., N-1, \quad m = 0, 1, ..., M-1$. We can note that (4.31) is the sum of L two-dimensional complex modes each of phase $\theta_\ell^{(t)}$ and $\theta_\ell^{(r)}$ and amplitude g_ℓ, hence by using the two-dimensional DFT of the channel matrix we can estimate the mode parameters. Actually we perform estimate of parameters by using the $N_B \times M_B$ submatrix:

$$\tilde{\mathbf{H}} = [\mathbf{H}]_{0:N_B-1, 0:M_B-1} \tag{4.32}$$

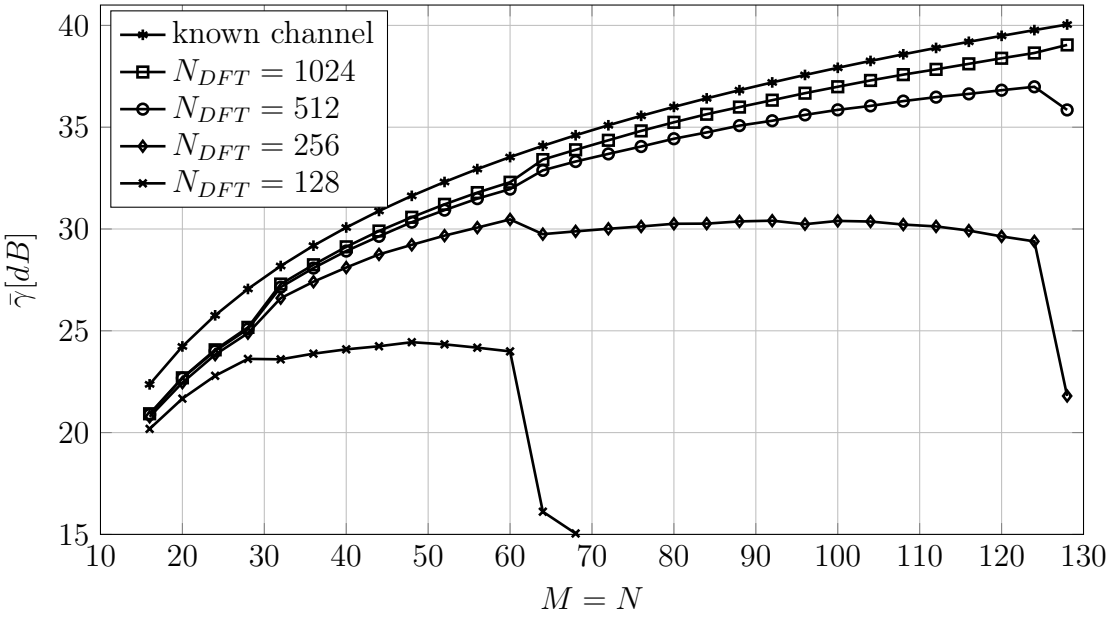

Figure 4.3: $\bar{\gamma}$ vs. M (and $M = N$) for the I-ADB algorithm in the presence of channel estimate with $M_D = N_D = 2^{\lfloor \log_2(M) \rfloor}$ for four values of N_{DFT} and $\Gamma_{AWGN} = 5dB$.

where N_B ($N_B \leq N$) and M_B ($M_B \leq M$) are two suitable integer parameters to be chosen. We can obtain $\tilde{\mathbf{H}}$ by stacking the following $N_{RF} \times M_{RF}$ submatrices

$$\begin{aligned} \tilde{\mathbf{H}}^{(p,q)} &= [\tilde{\mathbf{H}}]_{pN_{RF}:(p+1)N_{RF}-1, qM_{RF}:(q+1)M_{RF}-1} \\ & p = 0, 1, ..., \left\lceil \frac{N_B}{N_{RF}} \right\rceil - 1 \quad and \quad q = 0, 1, ..., \left\lceil \frac{M_B}{M_{RF}} \right\rceil - 1 \end{aligned} \tag{4.33}$$

In turn we obtain $\tilde{\mathbf{H}}^{(p,q)}$ by switching on only transmit antennas $qM_{RF}, ..., (q+1)M_{RF} - 1$, i.e. by setting

$$\mathbf{F}_{RF}^{(q)} = \begin{bmatrix} \mathbf{0} \\ \vdots \\ \mathbf{0} \\ \bar{\mathbf{F}}_{RF} \\ \mathbf{0} \\ \vdots \\ \mathbf{0} \end{bmatrix} \begin{matrix} \left.\begin{matrix} \\ \\ \\ \end{matrix}\right\} qM_{RF} \\ \\ \left.\begin{matrix} \\ \\ \\ \end{matrix}\right\} M - (q+1)M_{RF} \end{matrix} \qquad q = 0, 1, ..., \left\lceil \frac{M_B}{M_{RF}} \right\rceil - 1 \tag{4.34}$$

where $\bar{\mathbf{F}}_{RF}$ is a $M_{RF} \times M_{RF}$ square matrix, whose elements are chosen with unitary magnitude and such that $\bar{\mathbf{F}}_{RF}$ has full rank. At the same time we switch on only

receive antennas $pN_{RF}, ..., (p+1)N_{RF}-1$, i.e. by setting

$$\mathbf{U}_{RF}^{(p)} = \begin{bmatrix} \mathbf{0} \\ \vdots \\ \mathbf{0} \\ \bar{\mathbf{U}}_{RF} \\ \mathbf{0} \\ \vdots \\ \mathbf{0} \end{bmatrix} \begin{matrix} \left.\begin{matrix} \\ \\ \\ \end{matrix}\right\} pN_{RF} \\ \\ \left.\begin{matrix} \\ \\ \\ \end{matrix}\right\} N-(p+1)N_{RF} \end{matrix} \qquad p = 0, 1, ..., \left\lceil \frac{N_B}{N_{RF}} \right\rceil - 1 \tag{4.35}$$

where $\bar{\mathbf{U}}_{RF}$ is a $N_{RF} \times N_{RF}$ square matrix, whose elements are chosen with unitary magnitude and such that $\bar{\mathbf{U}}_{RF}$ has full rank. With these settings, we send a training sequence of vectors $\mathbf{x}_{BB}^{(m)}, \quad m = 0, 1, ..., M_{RF}-1$, where $\mathbf{x}_{BB}^{(m)}$ has $\frac{1}{\sqrt{M_{RF}}}$ in position m and zero otherwise. From (2.33) the base-band signal at the receiver becomes

$$\begin{aligned} \mathbf{y}_{BB}^{(p,q,m)} &= \left(\mathbf{U}_{RF}^{(p)}\right)^H \left(\mathbf{H}\mathbf{F}_{RF}^{(q)}\mathbf{x}_{BB}^{(m)} + \mathbf{n}^{(m)}\right) \\ &= \bar{\mathbf{U}}_{RF}^H \left(\tilde{\mathbf{H}}^{(p,q)}\bar{\mathbf{F}}_{RF}\mathbf{x}_{BB}^{(m)} + \bar{\mathbf{n}}^{(m)}\right), \quad m = 0, 1, ..., M_{RF}-1 \end{aligned} \tag{4.36}$$

where $\bar{\mathbf{n}}^{(m)} = [\mathbf{n}^{(m)}]_{qN_{RF}:(q+1)N_{RF}-1}$. From (4.36) we can estimate $\tilde{\mathbf{H}}^{(p,q)}$ by

$$\hat{\tilde{\mathbf{H}}}^{(p,q)} = \sqrt{M_{RF}} \left(\bar{\mathbf{U}}_{RF}^H\right)^{-1} [\mathbf{y}_{BB}^{(p,q,0)}, \mathbf{y}_{BB}^{(p,q,1)}, ..., \mathbf{y}_{BB}^{(p,q,M_{RF}-1)}](\bar{\mathbf{F}}_{RF})^{-1} \tag{4.37}$$

$$= \tilde{\mathbf{H}}^{(p,q)} + \tilde{\mathbf{n}} \tag{4.38}$$

where $\tilde{\mathbf{n}} = \sqrt{M_{RF}} \left[\bar{\mathbf{n}}^{(0)}, \bar{\mathbf{n}}^{(1)}, ..., \bar{\mathbf{n}}^{(M_{RF}-1)}\right] \left(\bar{\mathbf{F}}_{RF}\right)^{-1}$. To guarantee the full rank of matrices $\bar{\mathbf{F}}_{RF}$ and $\bar{\mathbf{U}}_{RF}$ we use Hadamard matrices [23] (see Appendix B). This guarantees also that the noise in (4.38) is still white with variance σ_n^2. If we probe all values of p and q in (4.37) we obtain an estimate $\hat{\tilde{\mathbf{H}}}$ of $\tilde{\mathbf{H}}$.

To estimate the parameters of complex modes we compute the 2D DFT of $\hat{\tilde{\mathbf{H}}}$ on $N_{DFT} \times N_{DFT}$ samples (set $[\hat{\tilde{\mathbf{H}}}]_{n,m} = 0$, for $n > N_B - 1$ and $m > M_B - 1$). If N_{DFT} is larger enough such that we can write

$$\theta_\ell^{(t)} = -2\pi \frac{i_\ell}{N_{DFT}}, \quad \theta_\ell^{(r)} = 2\pi \frac{k_\ell}{N_{DFT}} \tag{4.39}$$

the DFT of $\hat{\tilde{\mathbf{H}}}$ is

$$\begin{aligned} W(k,i) = DFT([\hat{\tilde{\mathbf{H}}}]_{n,m}) &= \frac{1}{M_B N_B} \sum_{m=0}^{N_{DFT}-1} \sum_{n=0}^{N_{DFT}-1} [\hat{\tilde{\mathbf{H}}}]_{n,m} e^{-j2\pi\left(\frac{im}{N_{DFT}} + \frac{kn}{N_{DFT}}\right)} \\ &= \frac{1}{M_B N_B} \sum_{m=0}^{M_B-1} \sum_{n=0}^{N_B-1} [\hat{\tilde{\mathbf{H}}}]_{n,m} e^{-j2\pi\left(\frac{im}{N_{DFT}} + \frac{kn}{N_{DFT}}\right)} \end{aligned} \tag{4.40}$$

Input:	$W(k,i), \quad k,i = 0,1,...,N_{DFT}-1$
1.	$W_1(k,i) = W(k,i)$
2.	**for** $\ell = 1$ **to** L
3.	$(\hat{k}_\ell, \hat{i}_\ell) = \arg\max_{k,i} \lvert W_\ell(k,i)\rvert$
4.	$\hat{g}_\ell = W_\ell(\hat{k}_\ell, \hat{i}_\ell)\sqrt{L}$
5.	$W_{\ell+1}(k,i) = W_\ell(k,i) - \frac{1}{\sqrt{L}}\hat{g}_\ell D(k-\hat{k}_\ell, i-\hat{i}_\ell)$
6.	**end for**

Table 4.2: Cancellation method to estimate the channel parameters.

for $k,i = 0,1,...,N_{DFT}-1$. Defined

$$d(n,m) = \begin{cases} \frac{1}{M_B N_B}, & 0 \le m < M_B, 0 \le n < N_B \\ 0, & otherwise \end{cases} \tag{4.41}$$

and

$$\begin{aligned} D(k,i) &= DFT\{d(n,m)\} \\ &= e^{-j\frac{2\pi k}{N_{DFT}}\frac{N_B-1}{2}} sinc_{N_B}\left(k\frac{N_B}{N_{DFT}}\right) e^{-j\frac{2\pi i}{N_{DFT}}\frac{M_B-1}{2}} sinc_{M_B}\left(i\frac{M_B}{N_{DFT}}\right) \end{aligned} \tag{4.42}$$

with $sinc_N(x) = \frac{\sin(\pi x)}{N\sin(\pi x/N)}$. From (4.31) and (4.38) it is

$$W(k,i) = \frac{1}{\sqrt{L}}\left[g_1 D(k-k_1, i-i_1) + \ldots + g_L D(k-k_L, i-i_L)\right] + N(k,i) \tag{4.43}$$

where $N(k,i) \sim \mathcal{CN}\left(0, \frac{\sigma_n^2}{N_B M_B}\right)$. We can estimate the parameters of different modes from $W(k,i)$ using the method outlined in Table 4.2. In practice also the number of modes L should be estimated by stopping the cancellation method when $|\hat{g}_i|$ turns out much smaller than $|\hat{g}_1|$. Here we simply assume that L is known. From $\hat{i}_\ell$ and $\hat{k}_\ell$ we can obtain $\hat{\phi}_\ell^{(t)}$ and $\hat{\phi}_\ell^{(r)}$ by (see (4.30) and (4.39))

$$\hat{\phi}_\ell^{(t)} = sin^{-1}\left(-\frac{2\pi\hat{i}_\ell}{\zeta D N_{DFT}}\right), \quad \hat{\phi}_\ell^{(r)} = sin^{-1}\left(\frac{2\pi\hat{k}_\ell}{\zeta D N_{DFT}}\right). \tag{4.44}$$

We note that this method needs a training sequence of

$$N_{TS} = \left\lceil \frac{N_B}{N_{RF}} \right\rceil \left\lceil \frac{M_B}{M_{RF}} \right\rceil M_{RF} \tag{4.45}$$

time slots.

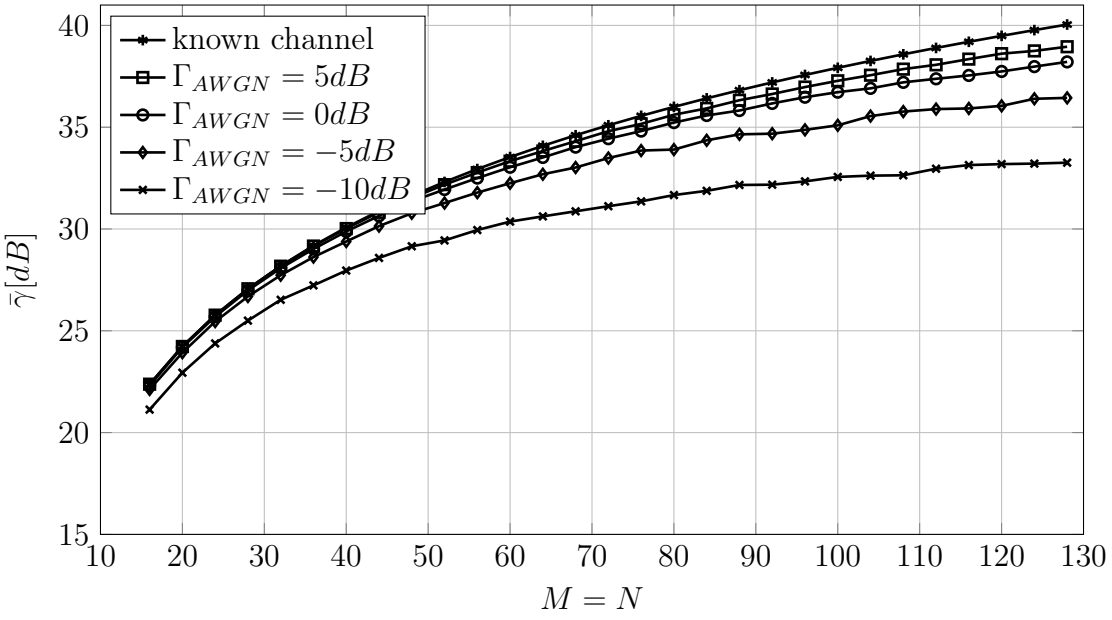

Figure 4.4: $\bar{\gamma}$ vs. M (and $M = N$) for the I-ADB algorithm in the presence of 2D channel estimate with $M_B = M_{RF} = N_B = N_{RF} = 16$ ($N_{TS} = M_{RF} = 16$).

4.2.2 Performance results

In this section, we present numerical results demonstrating the performance of the proposed channel estimate. Performance, in terms of $\bar{\gamma}$, are evaluated by averaging (2.36) for the same 5000 realizations of the channel. We apply the I-ADB algorithm to design the analog and digital precoders/beamformers with $N_I = 7$.
Figures 4.4 and 4.5 show the average SNR improvement $\bar{\gamma}$ versus the number of antennas $M = N$ for two values of $M_B = M_{RF} = N_B = N_{RF}$ and $N_{DFT} = 2048$. For a comparison we also report the performance bound by assuming the channel is known, when it is seen that $\bar{\gamma}$ is independent of the channel noise. We can see that performance using the channel estimate are close to the bound, especially for $M_B = M_{RF} = N_B = N_{RF} = 16$ (Fig. 4.4).
Moreover, performance are almost independent of M_{RF} (N_{RF}) if $M_{RF} > L$, and improve with M_D as from (4.43). Indeed higher value of M (N) require an higher M_B (N_B) to lower the noise level in the channel estimate.
In Fig. 4.6 we investigated the effect of N_{DFT} on the 2D estimate approach. For this we report $\bar{\gamma}$ versus the number of antennas for four value of N_{DFT}, $\Gamma_{AWGN} = 5dB$ and $M_B = M_{RF} = N_B = N_{RF} = 16$. We can see that for an higher number of antennas also N_{DFT} must increase, corresponding to a better accuracy in the angle estimate, otherwise performance deteriorate. In Fig. 4.7 we would compare the two estimate methods, for this we report $\bar{\gamma}$ versus the number of antennas $M = N$

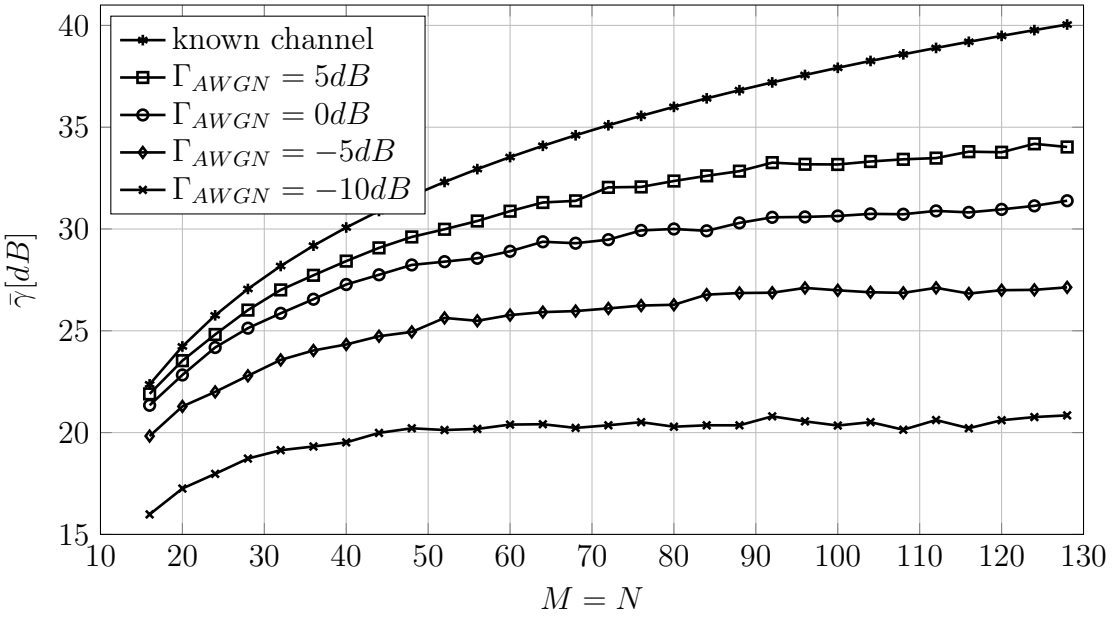

Figure 4.5: $\bar{\gamma}$ vs. M (and $M = N$) for the I-ADB algorithm in the presence of 2D channel estimate with $M_B = M_{RF} = N_B = N_{RF} = 8$ ($N_{TS} = M_{RF} = 8$).

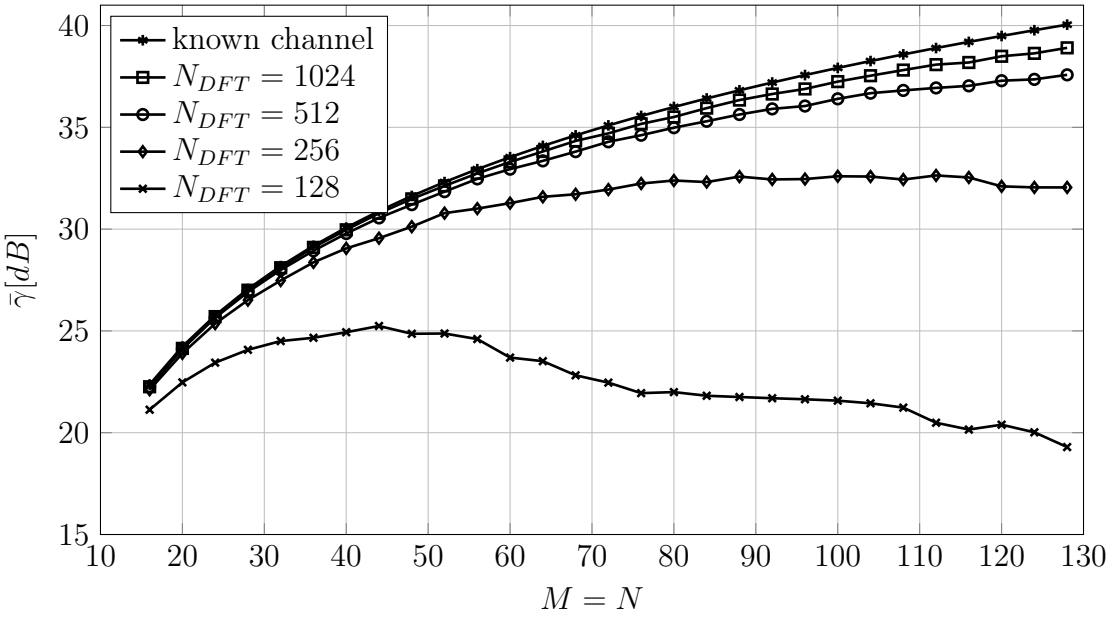

Figure 4.6: $\bar{\gamma}$ vs. M (and $M = N$) for the I-ADB algorithm in the presence of 2D channel estimate with $M_B = N_B = 16$ for four values of N_{DFT} and $\Gamma_{AWGN} = 5dB$.

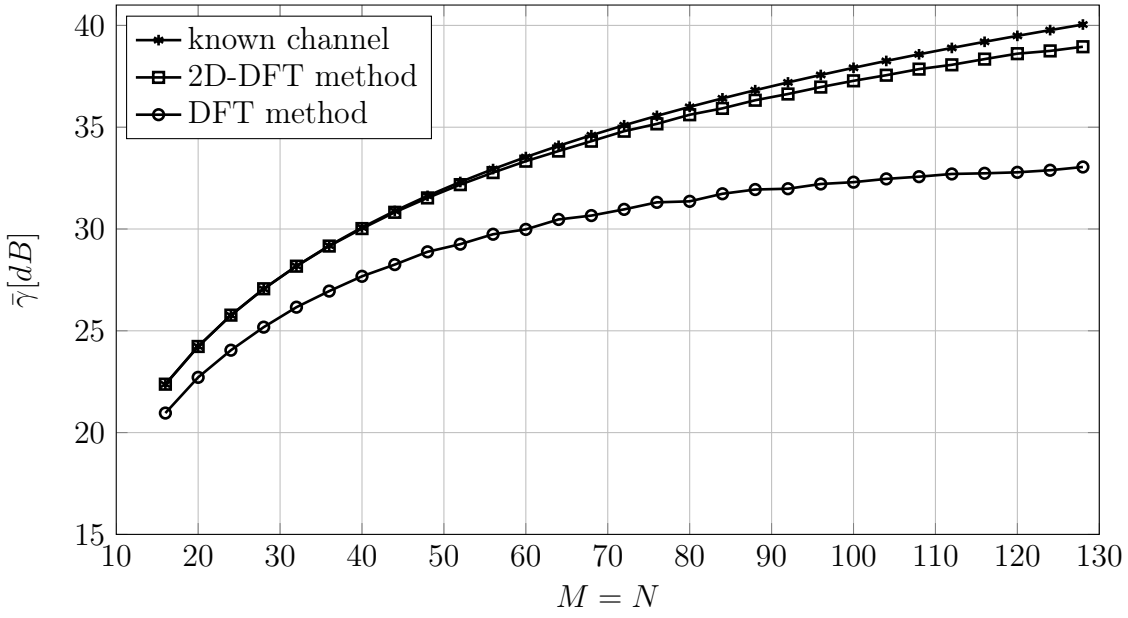

Figure 4.7: $\bar{\gamma}$ vs. M (and $M = N$) for the I-ADB algorithm in the presence of DFT and 2D-DFT channel estimate with $M_{RF} = N_{RF} = M_D = N_D = M_B = N_B = 16$, $N_{DFT} = 2048$ and $\Gamma_{AWGN} = 5dB$.

using $M_{RF} = N_{RF} = 16$, $N_{DFT} = 2048$ and $\Gamma_{AWGN} = 5dB$. In the both case we set $M_D = N_D = M_B = N_B = 16$, that correspond to have a length of training sequence equal to 17 time slots for the DFT estimate method and 16 time slots for the 2D-DFT method. We can see that the 2D-DFT method, using a shorter training sequence, achieves higher performance than the DFT estimate method at a cost of a greater computational complexity.

Chapter 5

Conclusion

We considered the problem of designing practical beamformers for MMW systems. Driven by the goal of reducing energy consumption, hardware costs and computational complexity we developed three iterative hybrid analog/digital beamforming algorithms (I-ADB, Q-ADB QI-ADB) for the MMW channel, one using the channel structure, in particular the ray phase vector response and two using vector quantization of the analog beamformers. We compared the proposed algorithms with the state-of-art fully analog and hybrid analog/digital ADB schemes. The simulation results showed that performance of the proposed algorithms can approximate the upper bound given the maximum-ratio-beamforming. In particular the QI-ADB algorithm with a high codebook size yields very good performance and has a computational complexity similar to that of ADB if M (and $N = M$) is sufficiently large. The I-ADB algorithm has the best performance, close to that ADB which, on the other hand, requires to know the channel structure, in particular the ray phase vector responses.
For the channel estimate, we developed two algorithms based on a training sequence of analog precoders/beamformers. In particular the algorithms estimate the parameters of the MMW channel rather than the channel matrix and account for the RF precoding/beamforming constraint. We evaluated the system performance in the presence of estimate channel and it is seen that our methods are a viable alternative to much more complex estimation methods which are based on an iterative feedback between receiver and transmitter.

Appendix A

Computational complexity of algorithms

We have evaluated expressions of the computational complexity in terms of number of complex multiplications for three algorithms.
We just observe that is our computational complexity, multiplication of a signal by a phasor (element with unitary amplitude) is evalueated by one complex multiplication. Indeed if special hardware is used complexity is much reduced.

A.1 ADB

As from the algorithm of Tab. 2.1 we report complexity of various steps for the design of transmit beamformer. Steps 5 and 6: $C_5 = C_6 = \mathcal{O}(L \cdot M)$. Step 8: $C_8 = \mathcal{O}(i^3 + 2 \cdot M \cdot i^2 + i \cdot M)$. Step 9: $C_9 = \mathcal{O}(2 \cdot i \cdot M + M)$. Step 11: $C_{11} = \mathcal{O}(M_{RF} \cdot M + M_{RF})$. The total design complexity is

$$\begin{aligned} C_{ADB,TX} =& \mathcal{O}\left(\sum_{i=1}^{M_{RF}} [C_5 + C_6 + C_8 + C_9] + C_{11}\right) \\ =& \mathcal{O}\Bigg(2 \cdot L \cdot [M \cdot M_{RF} + N \cdot N_{RF}] + \\ &+ \frac{M_{RF}^4}{4} + M_{RF}^3 \cdot \left[\frac{2}{3}M + \frac{1}{2}\right] + \\ &+ M_{RF}^2 \cdot \left[\frac{5}{2} \cdot M + \frac{1}{4}\right] + \\ &+ M_{RF} \cdot \left[\frac{23}{6} \cdot M + 1\right]\Bigg) \end{aligned} \tag{A.1}$$

Similarly, we can evaluate the complexity, $C_{ADB,RX}$, for the design of receive beamformer using N_{RF} and N instead of M_{RF} and M, respectively.
Complexity of the iterative procedure where transmit and receive beamformers are updated

$$C_{IT} = \mathcal{O}(N \cdot M_{RF}(M^2 + M_{RF})) \tag{A.2}$$

Complexity to evaluate $\boldsymbol{f}_{MRB}$ from $\mathbf{H}$ using SVD [20]

$$C_{SVD} = \mathcal{O}(2 \cdot N \cdot M^2 + 11 \cdot M^3) \tag{A.3}$$

The total complexity of the ADB algorithm is

$$\begin{aligned} C_{ADB} =& C_{ADB,TX} + C_{ADB,RX} + C_{IT} + C_{SVD} \\ =& \mathcal{O}(2 \cdot L \cdot [M \cdot M_{RF} + N \cdot N_{RF}] + \\ &+ \frac{M_{RF}^4}{4} + M_{RF}^3 \cdot \left[\frac{2}{3}M + \frac{1}{2}\right] + \\ &+ M_{RF}^2 \cdot \left[\frac{5}{2} \cdot M + \frac{1}{4}\right] + \\ &+ M_{RF} \cdot \left[\frac{23}{6} \cdot M + 1\right] + \frac{N_{RF}^4}{4} + \\ &+ N_{RF}^3 \cdot \left[\frac{2}{3} \cdot N + \frac{1}{2}\right] + \\ &+ N_{RF}^2 \cdot \left[\frac{5}{2} \cdot N + \frac{1}{4}\right] + \\ &+ N_{RF} \cdot \left[\frac{23}{6} \cdot N + 1\right] + \\ &+ N + M_{RF} \cdot \left[M^2 + M_{RF}\right] + \\ &+ 2 \cdot N \cdot M^2 + 11 \cdot M^3) \end{aligned} \tag{A.4}$$

A.2 I-ADB

As from the algorithm of Tab. 2.2 we report complexity of various steps for the design beamformers. Step 1: $C_1 = \mathcal{O}(N \cdot M \cdot N_{RF} + M \cdot N_{RF} \cdot M_{RF})$. Steps 4 and 6 : $C_4 = C_6 = \mathcal{O}(M_{RF} \cdot N_{RF})$. Step 5: $C_5 = \mathcal{O}(M_{RF})$. Step 7: $C_7 = \mathcal{O}(N_{RF})$. The total complexity of the I-ADB algorithm is

$$\begin{aligned} C_{I-ADB} =& C_1 + N_I(C_4 + C_5 + C_6 + C_7) \\ =& \mathcal{O}(N \cdot M \cdot N_{RF} + M \cdot N_{RF} \cdot M_{RF} + N_I \cdot (2 \cdot M_{RF} \cdot N_{RF} + M_{RF} + N_{RF})) \end{aligned} \tag{A.5}$$

A.3 Q-ADB

Complexity to design $\mathbf{F}_{RF}$ and $\mathbf{f}_{BB}$

$$C_{Q-ADB,TX} = \mathcal{O}(L_{TX}[M_{RF}(2 \cdot M + 1)]) \tag{A.6}$$

Complexity to design $\mathbf{U}_{RF}$ and $\mathbf{u}_{BB}$

$$C_{Q-ADB,RX} = \mathcal{O}(L_{RX}[N_{RF}(2 \cdot N + 1)]) \tag{A.7}$$

The total complexity of the Q-ADB algorithm is

$$\begin{aligned} C_{Q-ADB} =& C_{Q-ADB,TX} + C_{Q-ADB,RX} + \\ &+ C_{IT} + C_{SVD} \\ =& \mathcal{O}(L_{TX} \cdot [M_{RF} \cdot (2 \cdot M + 1)] + \\ &+ L_{RX} \cdot [N_{RF} \cdot (2 \cdot N + 1)] + \\ &+ N \cdot M_{RF} \cdot \left(M^2 + M_{RF}\right) + \\ &+ 2 \cdot N \cdot M^2 + 11 \cdot M^3) \end{aligned} \tag{A.8}$$

A.4 QI-ADB

As from the algorithm of Tab. 3.2 we report complexity of various steps for the design beamformers. Steps 4 : $C_4 = \mathcal{O}(M \cdot N + N \cdot N_{RF})$. Step 5: $C_5 = \mathcal{O}(N_I \cdot [2 \cdot M_{RF} \cdot N_{RF} + M_{RF} + N_{RF}])$. Complexity to normalize $\mathbf{f}_{BB}$ and $\mathbf{u}_{BB}$

$$C_{NORM} = \mathcal{O}(M_{RF} + N_{RF}) \tag{A.9}$$

The total complexity of the QI-ADB algorithm is

$$\begin{aligned} C_{QI-ADB} =& L_{TX} \cdot L_{RX}[C_4 + C_5 + C_{NORM}] \\ =& \mathcal{O}(L_{TX} \cdot L_{RX} \cdot [M \cdot N + N \cdot N_{RF} + \\ &+ N_I \cdot (2 \cdot M_{RF} \cdot N_{RF} + M_{RF} + N_{RF}) + \\ &+ M_{RF} + N_{RF}]) \end{aligned} \tag{A.10}$$

Appendix B

Hadamard matrices

Hadamard matrix [23] is a square matrix of length 2^m whose entries are either $+1$ or -1 and whose rows are mutually orthogonal. Let $\mathbf{A}_m$ be a Hadamard matrix of order m. The transpose of $\mathbf{A}_m$ is closely related to its inverse as

$$\mathbf{A}_m^T \mathbf{A}_m = m\mathbf{I}_m \tag{B.1}$$

We consider $2^m \times 2^m$ Hadamard matrices $\mathbf{A}_m$, for the first orders, we have

$$\mathbf{A}_0 = [1] \qquad \mathbf{A}_1 = \begin{bmatrix} 1 & 1 \\ 1 & -1 \end{bmatrix} \tag{B.2}$$

In general the construction is recursive

$$\mathbf{A}_m = \begin{bmatrix} \mathbf{A}_{m-1} & \mathbf{A}_{m-1} \\ \mathbf{A}_{m-1} & -\mathbf{A}_{m-1} \end{bmatrix} \tag{B.3}$$

Bibliography

[1] Z. Pi and F. Khan, "An introduction to millimeter-wave mobile broadband systems", *IEEE Communication Magazine*, vol. 49, no. 6, pp. 101-107, 2011.

[2] Sundeep Rangan, Theodore S. Rappaport and Elza Erkip "Millimeter-Wave Cellular Wireless Networks: Potentials and Challenges," *Proceedings of the IEEE*, vol. 102, no. 3, March 2014.

[3] Standard ECMA-387, "High rate 60Ghz PHY,MAC and HDMI PAL.," [Online] Available: www.ecma-international.org/

[4] C. Doan, S. Emami, D. Sobel, A. Niknejad, and R. Brodersen, "Design considerations for 60 GHz CMOS radios," *IEEE Communications Magazine,* vol. 42, no. 12, pp. 132-140, 2004.

[5] R. Eickhoff, R. Kraemer, I. Santamaria, and L. Gonzalez, "Integrated low power RF-MIMO transceiver for enhanced 802.11a short-range communication," *IEEE Veh. Technol. Mag.* , vol. 4, no. 1, pp. 34âĂŞ41, Mar. 2009.

[6] F. Gholam, J. Via, and I. Santamaria, "BEamforming design for simplified analog antenna combining architectures," *IEEE Transactions on Vehicular Technology* vol. 60, no. 5. pp. 2373-2378, 2011.

[7] S. Rajagopal, S. Abu-Surra, Z. Pi, and F. Khan , "Antenna array design for multi-gbps mm-wave mobile broadband communication," *IEEE Global Telecommunications Conference (GLOBECOM),* pp. 1-6, 2011.

[8] O. Ayach, R. Heath, S. Abu-Surra, S. Rajagopal, and Z. Pi, "Low complexity precoding for large millimeter wave mimo systems," *IEEE International Conference on Communication (ICC),* Ottawa, ON, pp. 3724-3729, 2012.

[9] Ahmed Alkhateeb, Omar El Ayach, Geert Leus, and Robert W. Heath Jr. "Channel Estimation and Hybrid Precoding for Millimeter Wave Cellular Systems," arXiv:1401.7426v1, 29 Jan 2014.

[10] David J. Love, Robert W. Heath, " Equal Gain Transmission in Multiple-Input Multiple-Output Wireless Systems", *TCOM* 2003.

[11] M. Biguesh, and A.B. Gershman "Training-based MIMO channel estimation: a study of estimator tradeoffs and optimal training signals," *Signal Processing, IEEE Transactions*, vol. 54 , no. 3, pp. 884 - 893, March 2006

[12] K. Yu, "Modeling of multiple-input multiple-output radio propagation channels," PhD thesis, 2002.

[13] X. Zheng, Y. Xie, J. Li, and P. Stoica, "Mimo transmit beamforming under uniform elemental power constraint," *IEEE Transactions on Signal Processing*, vol. 55, no. 11, pp. 5395-5406, 2007.

[14] T. Lo, "Maximum ratio transmission," *IEEE Transactions on Communications*, vol. 47, no. 10, pp. 1458-1461, 1999.

[15] A. Paulraj, R. Nabar, and D. Gore, "Introduction to Space-Time Wireless Communications," Cambridge University Press, 2003.

[16] A. Gersho and R. M. Gray, "Vector quantization and signal compression," Boston, MA: Kluwer Academic Publishers, 1992.

[17] R. M. Gray, "Vector quantization", *IEEE ASSP Magazine*, vol. 1, pp. 4-29, Apr. 1984.

[18] Y. Linde, A. Buzo, and R. M. Gray, "An algorithm for vector quantizer design", *IEEE Trans. on Communications*, vol. 28, pp. 84-95, Jan. 1980.

[19] V. Raghavan, and A. Sayeed, "Multi-antenna capacity of sparse multipath channels," submitted to *IEEE Trans. Inform. Theory,* Aug. 2006. [Online] Available: dune.ece.wisc.edu/pdfs/sp_mimo_cap.pdf

[20] G. H. Golub, C. F. Van Loan, "Matrix Computations," *The Johns Hopkins Univ. Press*, Ed., 1996.

[21] N. Belli, " Mimo Array Gain Techniques for Communications over mm-wave Channels", *Master's thesis, Università degli Studi di Padova*, 2013.

[22] L. Pilloni, " Tecniche di beamforming in canali MIMO ad onde millimetriche", Master's thesis, *Università degli Studi di Padova*, 2013.

[23] N. Benvenuto, G. Cherubini, " Algorithms for Communications Systems and their Applications", Wiley, Ed., 2003.